JOURNAL OF GEOPHYSICAL RESEARCH, VOL. 95, NO. B13, PAGES 21,965–21,981, DECEMBER 10, 1990

Pacific-North America Plate Motions: New Results From Very Long Baseline Interferometry

STEVEN N. WARD

C. F. Richter Laboratory, Institute of Tectonics, University of California, Santa Cruz

Expansion and densification of the very long baseline interferometry (VLBI) network by the NASA Crustal Dynamics Project continues to clarify details of Pacific-North America motions. In this paper I construct, for the first time, rigid plate tectonic models based purely on space geodetic data. Construction of VLBI plate models has the advantages of averaging the bias and errors of individual site velocities, making failures in the rigid plate assumption easy to document, and allowing the consistency of specified plate models to be quantified against the VLBI data set as a whole. VLBI-based rigid plate models VM2 and VM3, obtained by fitting vector velocities of 10 sites in the stable interiors of the North America and Pacific plates, reveal a misfit of VLBI observations and RM2 (Minster and Jordan, 1978) predictions significant at the 99% confidence level. NUVEL 1 (DeMets et al., 1990) reproduces the velocities of these 10 sites far better than RM2 and offers a fit to the data which is statistically indistinguishable from VM2 and VM3. By including velocities of 16 additional stations in the deforming plate margin, VM2 and VM3 can resolve all four terms ($\mathbf{V}_{PN}$, total Pacific-North America motion, $\mathbf{V}_{SA}$, San Andreas slip, $\mathbf{V}_{E,W}$, path integrated deformation east and west of the San Andreas) in the vector equation characterizing Pacific-North America plate boundary deformation: $\mathbf{V}_{PN} - \mathbf{V}_{SA} = \mathbf{V}_E - \mathbf{V}_W$ for several points along the San Andreas without reference to a global plate model, geological or local geodetic measurements, or restrictions on distributed shear. In most cases, instantaneous VLBI-determined rates agree with geologically based estimates. Mapped to point C (36.0°N, 120.6°W) in central California, VM2 gives $\mathbf{V}_{PN}(\mathbf{C})$= 46.8±1.4 mm/yr (N36°±2°W), $\mathbf{V}_{SA}(\mathbf{C})$= 38.6±1.3 mm/yr (N36°±2°W), and $\mathbf{V}_E(\mathbf{C})$= 8.2±1.3 mm/yr (N34°±7°W). VLBI substantially eliminates $\mathbf{V}_W(\mathbf{C})$, the component of the San Andreas Discrepancy west of C, although a few millimeters per year of right-lateral strike slip on offshore faults can not be rejected. At point D (34.1°N, 117.0°W) in southern California, VM2 returns $\mathbf{V}_{SA}(\mathbf{D})$= 25.0±1.1 mm/yr (N52°±3°W), $\mathbf{V}_E(\mathbf{D})$= 8.8±1.1 mm/yr (N25°±8°W), and $\mathbf{V}_W(\mathbf{D})$= 13.3±1.6 mm/yr (N21°±5°W). $\mathbf{V}_W(\mathbf{D})$ is accommodated west of the San Andreas to the Channel Islands. The azimuth of San Andreas slip suggests that the transverse ranges north of Los Angeles are absorbing 8±1 mm/yr of compression perpendicular to the trend of the fault.

INTRODUCTION

As of February 1989, the NASA Crustal Dynamics Project had assembled very long baseline interferometry (VLBI) measurements of length and transverse velocity along 113 baselines in North America and around the Pacific Rim (Figure 1 and Tables 1 and 2). The network connects 27 stations, 21 of which lie in the western United States. The remaining sites include Westford, Massachusetts; Fairbanks, Alaska; Kashima, Japan; Kwajalein, Marshall Islands; and Kauai, Hawaii. These lines have been surveyed between 3 and 126 times over an eight year period. Standard errors in the measured velocities are 0.3 - 23.2 mm/yr, with a median of 2.1 mm/yr (D. Gordon, personal communication, 1989).

Elucidating Pacific-North America plate motion has been a goal of the VLBI project since its inception [*Coates et al.*, 1985]. Until recently, however, lack of sufficient data fostered two areas of confusion. First, it had been difficult to identify "stable" North America from which to reference Pacific plate rates. Second, absence of VLBI sites west of the North American continent made definitive measurements of relative motion impossible because it was uncertain whether California coastal stations like Vandenberg and Ft. Ord were firmly fixed to the Pacific plate.

Now, thanks to recent densification, expansion, and improvements, the VLBI network provides data which c[illegible] these issues. This note updates the state of Pacific-North America interaction in light of the newest VLBI measurements by addressing three questions: (1) What is the relative motion between the Pacific and North American plates as measured from their stable interiors? (2) Is there evidence of Pacific plate deformation off the central California coast? (3) How is path integrated deformation distributed east of the San Andreas fault? Answers to these questions have implications ranging from lithospheric rheology to earthquake hazard.

CHARACTERIZATION OF PLATE BOUNDARY DEFORMATION

Consider points N and P in the stable interiors of the North American and Pacific plates (Figure 2). Let a path connecting the points run through the western North America margin and contain point C on the San Andreas fault in central California. *Minster and Jordan* [1984] characterized plate boundary deformation along path NP with the simple vector equation

$$\mathbf{V}_{PN}(\mathbf{C}) - \mathbf{V}_{SA}(\mathbf{C}) = \mathbf{V}_E(\mathbf{C}) - \mathbf{V}_W(\mathbf{C}) \quad (1)$$

where

$$\mathbf{V}_{PN}(\mathbf{C}) = [\Omega_{PAC} - \Omega_{NAM}] \times \mathbf{C} \quad (2)$$

Paper number 90JB01756.
0148-0227/90/90JB-01756$05.00

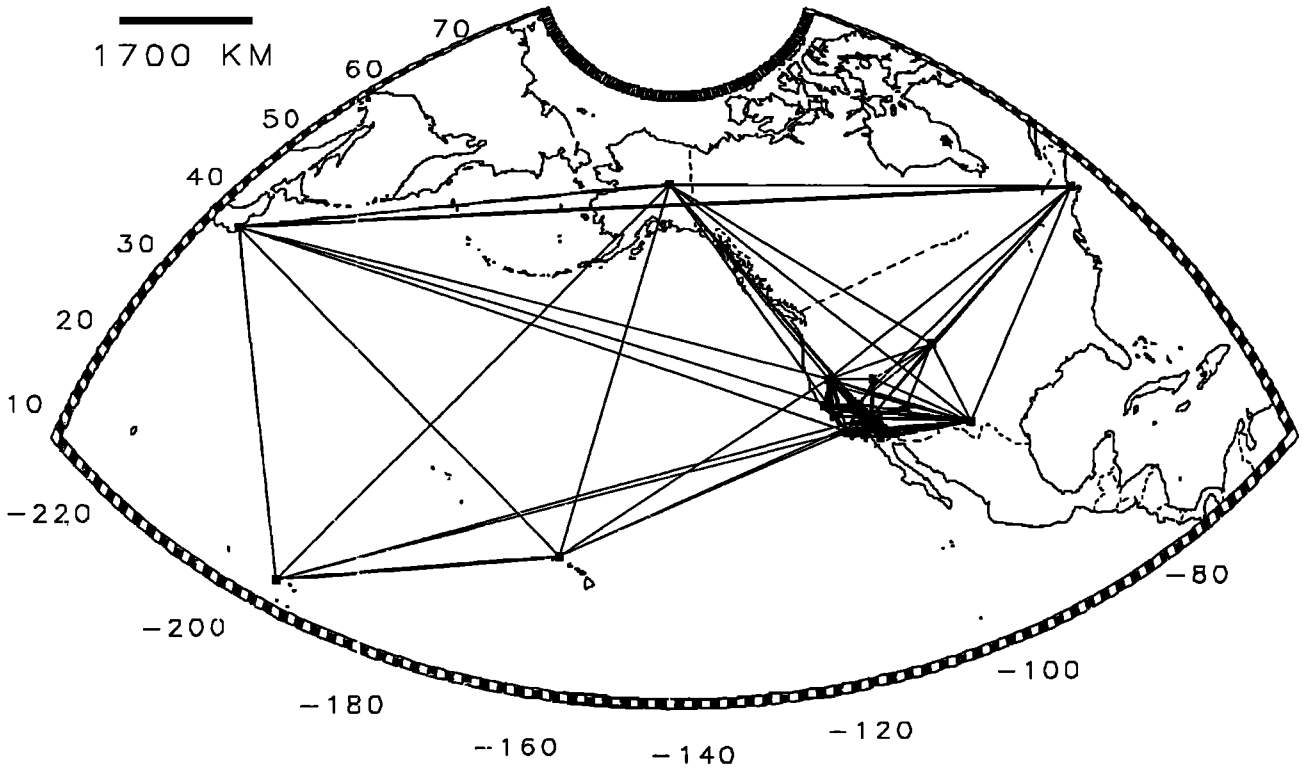

Fig. 1. Map illustrating the 113 VLBI baselines employed in this paper. The dense network in the far western United States provides a detailed picture of plate boundary deformation. Sites elsewhere in stable North America and the mid-Pacific provide estimates of relative plate motion unbiased by plate boundary deformation.

TABLE 1. Baseline Data Employed in This Paper

Station Pair		Velocity-Length				Velocity-Transverse			
		Rate, mm/yr	σ, mm/yr	Number of Points	Epoch	Rate mm/yr	σ, mm/yr	Number of Points	Epoch
MOJAVE	VNDNBERG	17.7	0.5	126	83.7-89.1	35.6	0.4	117	84.2-89.1
MOJAVE	OVRO	1.6	0.5	71	83.5-88.9	-0.8	0.6	61	84.2-88.9
MOJAVE	FT.DAVIS	4.3	0.5	98	83.5-88.9	7.0	0.7	93	84.3-88.9
MOJAVE	HATCREEK	-0.8	0.6	85	83.5-89.1	-2.8	0.6	83	84.2-89.1
MOJAVE	FAIRBNKS	-8.6	0.8	98	84.5-89.1	-0.4	1.3	98	84.5-89.1
MOJAVE	WESTFORD	-3.1	1.2	64	84.3-88.9	12.6	2.0	64	84.3-88.9
MOJAVE	MONPEAK	-22.5	1.2	28	83.5-88.8	24.8	1.3	25	84.3-88.8
MOJAVE	JPL	4.0	1.4	21	83.5-88.9	27.1	0.8	17	84.2-88.9
MOJAVE	PLATTVIL	-2.2	1.1	17	84.3-88.8	11.3	1.4	17	84.3-88.8
MOJAVE	PINFLATS	-12.8	1.0	19	83.8-88.4	11.1	1.1	17	84.8-88.4
MOJAVE	YUMA	7.9	1.2	21	83.8-88.8	2.0	1.1	19	84.8-88.8
MOJAVE	PRESIDIO	22.3	1.7	16	83.7-89.1	9.4	2.0	14	85.2-89.1
MOJAVE	QUINCY	2.7	2.0	11	83.5-88.8	-4.8	1.7	10	84.3-88.8
MOJAVE	BLKBUTTE	3.3	1.8	12	83.8-88.8	5.4	0.9	10	84.2-88.8
MOJAVE	PBLOSSOM	2.3	2.0	9	83.7-88.1	17.2	1.1	8	84.2-88.1
MOJAVE	PT.REYES	28.5	1.6	12	83.7-89.1	16.0	1.9	11	84.2-89.1
MOJAVE	FT.ORD	32.9	1.6	11	83.7-88.2	24.3	2.1	10	84.2-88.2
MOJAVE	FLAGSTAF	3.3	1.8	6	84.3-88.8	9.4	2.5	6	84.3-88.8
MOJAVE	ELY	-6.0	1.7	8	84.3-88.8	3.2	1.3	8	84.3-88.8
MOJAVE	SANPAULA	13.8	2.8	8	83.7-89.1	25.6	2.2	7	84.2-89.1
MOJAVE	DEADMANL	0.6	6.2	5	84.2-88.1	4.4	4.1	5	84.2-88.1
MOJAVE	PVERDES	-4.6	2.4	7	83.9-89.1	30.2	1.4	6	85.2-89.1
MOJAVE	MAMMOTHL	4.0	2.5	4	83.5-86.8	-6.8	4.5	3	84.3-86.8
OVRO	WESTFORD	3.3	0.6	55	80.3-88.8	8.6	3.0	20	84.3-88.8
OVRO	VNDNBERG	-9.1	1.0	46	83.7-88.9	37.8	1.0	40	84.2-88.9
OVRO	FT.DAVIS	7.4	0.3	73	80.3-88.8	5.6	1.6	40	84.3-88.8
OVRO	HATCREEK	-1.9	0.9	31	83.5-88.9	-3.1	0.9	28	84.2-88.9
OVRO	FAIRBNKS	-16.6	3.3	11	85.4-88.9	-4.3	4.9	11	85.4-88.9
OVRO	JPL	-10.8	4.6	19	82.8-88.9	19.6	1.4	13	84.2-88.9
OVRO	MONPEAK	-26.1	1.1	18	82.8-88.8	20.0	1.7	14	84.3-88.8

TABLE 1. (continued)

Station Pair		Velocity-Length				Velocity-Transverse			
		Rate, mm/yr	σ, mm/yr	Number of Points	Epoch	Rate mm/yr	σ, mm/yr	Number of Points	Epoch
OVRO	PRESIDIO	17.9	1.9	10	83.7-88.8	12.4	2.3	8	84.2-88.8
OVRO	PBLOSSOM	-8.5	3.3	7	83.2-87.8	12.9	1.1	5	84.2-87.8
OVRO	QUINCY	0.9	2.1	11	82.8-88.8	-2.7	1.7	8	84.3-88.8
OVRO	PLATTVIL	1.8	3.0	8	84.3-88.3	13.8	0.9	8	84.3-88.3
OVRO	PINFLATS	-13.1	1.8	7	83.8-86.8	8.1	5.3	6	84.8-86.8
OVRO	YUMA	3.1	2.1	7	83.8-87.8	5.3	3.9	6	85.2-87.8
OVRO	PT.REYES	24.3	3.1	6	83.7-88.8	21.0	6.4	5	84.2-88.8
OVRO	FT.ORD	13.8	0.6	5	83.7-87.8	41.8	11.3	4	84.2-87.8
OVRO	BLKBUTTE	-1.8	15.6	3	86.4-87.8	20.5	16.0	3	86.4-87.8
OVRO	MAMMOTHL	3.3	2.8	4	83.5-86.8	-4.1	2.0	3	84.3-86.8
VNDNBERG	FAIRBNKS	-45.6	2.2	49	84.5-89.1	16.8	1.8	49	84.5-89.1
VNDNBERG	FT.DAVIS	36.3	1.2	38	83.8-88.8	30.4	1.5	37	84.3-88.8
VNDNBERG	HATCREEK	-34.3	1.0	60	84.2-89.1	21.7	1.0	60	84.2-89.1
VNDNBERG	JPL	10.3	1.6	18	83.7-88.9	13.2	1.8	16	84.2-88.9
VNDNBERG	MONPEAK	4.7	2.1	22	83.8-88.8	14.2	1.9	21	84.3-88.8
VNDNBERG	PINFLATS	15.9	1.3	18	83.8-88.4	16.9	1.8	16	84.8-88.4
VNDNBERG	YUMA	39.3	1.7	19	83.8-88.8	26.9	1.8	18	84.8-88.8
VNDNBERG	ELY	-0.5	7.5	5	87.4-88.8	49.4	8.8	5	87.4-88.8
VNDNBERG	PRESIDIO	-13.7	1.8	16	83.7-89.1	3.2	2.1	14	84.2-89.1
VNDNBERG	PBLOSSOM	15.6	2.0	9	83.7-88.1	16.6	0.7	8	84.2-88.1
VNDNBERG	BLKBUTTE	28.9	1.8	12	83.8-88.8	29.5	1.7	10	84.2-88.8
VNDNBERG	FT.ORD	0.9	1.6	11	83.7-88.2	5.6	2.2	10	84.2-88.2
VNDNBERG	PT.REYES	-4.8	1.4	12	83.7-89.1	6.2	1.7	11	84.2-89.1
VNDNBERG	QUINCY	-30.7	2.3	9	84.3-88.8	19.7	2.3	9	84.3-88.8
VNDNBERG	SANPAULA	-3.0	5.3	8	83.7-89.1	15.5	1.6	7	84.2-89.1
VNDNBERG	DEADMANL	17.2	14.4	5	84.2-88.1	29.7	7.0	5	84.2-88.1
VNDNBERG	PVERDES	4.8	2.2	7	83.9-89.1	11.1	2.4	6	85.2-89.1
HATCREEK	FT.DAVIS	8.0	0.9	50	83.5-88.8	1.5	1.3	46	84.3-88.8
HATCREEK	FAIRBNKS	-7.8	2.1	32	85.4-89.1	3.3	2.8	32	85.4-89.1
HATCREEK	WESTFORD	9.8	3.3	10	83.5-88.3	10.7	3.5	8	84.3-88.3
HATCREEK	PLATTVIL	5.0	1.5	17	83.5-88.8	7.1	1.4	16	84.3-88.8
HATCREEK	MONPEAK	-29.1	1.9	16	83.5-88.8	15.0	2.2	15	84.3-88.8
HATCREEK	PRESIDIO	-14.4	2.7	11	84.2-89.1	17.0	2.8	11	84.2-89.1
HATCREEK	QUINCY	-2.5	1.3	8	83.5-88.8	2.3	2.0	7	84.3-88.8
HATCREEK	FT.ORD	-31.4	4.0	10	84.2-88.2	24.3	3.3	10	84.2-88.2
HATCREEK	FLAGSTAF	8.1	1.9	6	84.3-88.8	8.0	2.1	6	84.3-88.8
HATCREEK	PT.REYES	-19.5	2.7	10	84.2-89.1	27.2	1.3	10	84.2-89.1
HATCREEK	YUMA	10.0	3.4	12	85.2-88.8	0.7	2.4	12	85.2-88.8
HATCREEK	ELY	4.5	2.6	7	85.4-88.8	0.7	3.6	7	85.4-88.8
HATCREEK	BLKBUTTE	-1.2	10.5	5	87.1-88.8	-1.0	4.6	5	87.1-88.8
FT.DAVIS	WESTFORD	-0.6	0.5	75	80.3-88.9	2.1	1.9	42	84.3-88.9
FT.DAVIS	FAIRBNKS	0.5	2.6	31	84.7-88.9	-5.7	3.1	31	84.7-88.9
FT.DAVIS	MONPEAK	34.6	1.0	29	82.8-88.8	18.7	2.1	24	84.3-88.8
FT.DAVIS	PLATTVIL	-0.4	1.2	18	83.5-88.8	1.6	1.5	17	84.3-88.8
FT.DAVIS	PINFLATS	22.0	1.8	5	85.8-86.9	20.0	5.8	5	85.8-86.9
FT.DAVIS	YUMA	2.4	1.6	18	83.8-88.8	1.5	2.1	17	85.2-88.8
FT.DAVIS	PRESIDIO	31.3	12.5	5	85.2-87.1	18.8	3.7	5	85.2-87.1
FT.DAVIS	QUINCY	8.9	2.7	12	82.8-88.8	0.3	3.4	10	84.3-88.8
FT.DAVIS	FT.ORD	28.9	2.5	4	85.2-87.8	29.2	5.8	4	85.2-87.8
FT.DAVIS	FLAGSTAF	2.9	2.9	6	84.3-88.8	2.2	5.0	6	84.3-88.8
FT.DAVIS	ELY	3.3	2.3	8	84.3-88.8	-1.3	1.3	8	84.3-88.8
FT.DAVIS	BLKBUTTE	7.3	3.4	5	83.8-88.8	2.7	5.0	4	86.4-88.8
FT.DAVIS	JPL	34.9	12.1	3	82.8-87.8	-	-	-	-
WESTFORD	FAIRBNKS	3.1	1.8	48	84.7-88.9	2.4	2.9	48	84.7-88.9
WESTFORD	PLATTVIL	5.8	3.9	8	83.5-88.3	1.5	2.9	7	84.3-88.3
FAIRBNKS	PLATTVIL	1.8	6.2	6	85.4-88.3	-0.5	8.8	6	85.4-88.3
MONPEAK	QUINCY	-26.9	3.1	11	83.5-88.8	12.9	2.1	10	84.3-88.8
MONPEAK	YUMA	27.6	2.1	8	83.8-87.9	23.4	4.1	7	85.2-87.9
MONPEAK	BLKBUTTE	2.2	5.8	4	83.8-86.8	26.6	9.4	3	85.0-86.8
PLATTVIL	FLAGSTAF	6.2	1.9	4	84.3-88.8	0.2	0.9	4	84.3-88.8
PLATTVIL	ELY	6.6	12.6	3	84.3-86.3	-4.2	4.4	3	84.3-86.3
FT.ORD	PRESIDIO	-10.9	3.6	5	83.7-88.2	1.2	5.5	4	85.2-88.2
JPL	PBLOSSOM	-2.2	1.2	7	83.2-88.0	9.3	2.1	5	84.2-88.0
JPL	PINFLATS	4.6	3.1	6	83.8-87.0	12.3	2.0	5	85.0-87.0
JPL	MAMMOTHL	-16.0	9.2	4	83.5-86.8	3.0	2.9	3	84.3-86.8
YUMA	PINFLATS	24.0	5.2	6	83.8-86.9	14.5	7.5	5	84.8-86.9
PT.REYES	PRESIDIO	2.4	2.0	4	83.7-85.8	8.4	23.2	3	84.2-85.8
SANPAULA	DEADMANL	32.8	5.6	4	84.2-87.9	10.4	5.9	4	84.2-87.9
MOJAVE	KAUAI	18.4	1.4	34	84.5-88.8	71.7	2.1	34	84.5-88.8
MOJAVE	KASHIMA	-6.4	2.3	33	84.6-88.9	17.9	4.8	33	84.6-88.9
MOJAVE	KWAJLEIN	14.9	3.7	17	84.5-88.6	74.0	5.7	17	84.5-88.6

TABLE 1. (continued)

Station Pair		Velocity-Length				Velocity-Transverse			
		Rate, mm/yr	σ, mm/yr	Number of Points	Epoch	Rate mm/yr	σ, mm/yr	Number of Points	Epoch
HATCREEK	KAUAI	-0.7	2.4	12	85.4-88.8	80.2	4.8	12	85.4-88.8
HATCREEK	KASHIMA	-14.3	2.8	12	85.4-88.8	18.8	7.9	12	85.4-88.8
VNDNBERG	KAUAI	-4.0	2.8	25	84.5-88.8	40.6	3.1	25	84.5-88.8
VNDNBERG	KASHIMA	-35.4	6.1	20	85.4-88.8	9.0	6.2	20	85.4-88.8
VNDNBERG	KWAJLEIN	-1.8	6.6	12	84.5-88.6	37.9	10.4	12	84.5-88.6
FAIRBNKS	KAUAI	-46.0	1.3	55	84.5-89.1	67.4	2.3	55	84.5-89.1
FAIRBNKS	KASHIMA	1.0	1.5	62	84.6-89.1	19.1	2.8	62	84.6-89.1
FAIRBNKS	KWAJLEIN	-22.8	3.6	19	84.5-88.6	91.3	4.4	19	84.5-88.6
KAUAI	KASHIMA	-65.1	1.7	48	84.6-89.1	-9.9	3.0	48	84.6-89.1
KAUAI	KWAJLEIN	0.3	2.4	20	84.5-88.6	7.7	2.9	20	84.5-88.6
KASHIMA	KWAJLEIN	-68.9	2.1	16	84.6-88.6	29.9	3.9	16	84.6-88.6
KASHIMA	WESTFORD	-15.3	15.3	9	84.6-88.9	43.0	11.2	9	84.6-88.9

GLB511, June 14, 1989, D. Gordon NASA-GSFC. Transverse rates are tied to the Polaris-IRIS earth orientation series derived under the assumption that the azimuth from Westford MA to Richmond FL is fixed.

TABLE 2. VLBI Site Names and Locations

Site	Location	Latitude °N	Longitude °E
FAIRBNKS	Fairbanks, Alaska	64.98	212.51
HATCREEK	Hatcreek, California	40.82	238.53
KASHIMA	Kashima, Japan	35.95	140.67
KAUAI	Kauai, Hawaii	22.13	200.33
KWAJLEIN	Kwajalein, Marshall Islands	9.40	167.48
MOJAVE	Barstow, California	35.33	243.11
VNDNBERG	Vandenberg, California	34.56	239.38
BLKBUTTE	Black Butte, California	33.66	244.28
DEADMANL	Deadman Lake, California	34.25	243.72
ELY	Ely, Nevada	39.29	245.16
FLAGSTAF	Flagstaff, Arizona	35.21	248.37
FT.DAVIS	Fort Davis, Texas	30.64	256.05
FT.ORD	Fort Ord, California	36.67	238.23
JPL	Pasadena, California	34.21	241.83
MAMMOTHL	Mammoth Lakes, California	37.64	241.06
MONPEAK	Monument Peak, California	32.89	243.58
OVRO	Owens Valley, California	37.23	241.71
PBLOSSOM	Pearblossom, California	34.51	242.08
PINFLATS	Pinyon Flat, California	33.61	243.54
PLATTVIL	Platteville, Colorado	40.18	255.27
PT.REYES	Point Reyes, California	38.10	237.06
PRESIDIO	San Francisco, California	37.81	237.55
PVERDES	Palos Verdes, California	33.74	241.60
QUINCY	Quincy, California	39.98	239.06
SANPAULA	Santa Paula, California	34.39	241.00
WESTFORD	Westford, Massachusetts	42.61	288.51
YUMA	Yuma, Arizona	32.94	245.80

$$\mathbf{V}_E(\mathbf{C}) = \int_{\mathbf{N}}^{\mathbf{C}} d\mathbf{s} \cdot \nabla_s \mathbf{V}(\mathbf{s}) + \boldsymbol{\Omega}_{NAM} \times (\mathbf{N} - \mathbf{C}) = [\boldsymbol{\Omega}_E(\mathbf{C}) - \boldsymbol{\Omega}_{NAM}] \times \mathbf{C} \quad (3)$$

$$\mathbf{V}_W(\mathbf{C}) = \int_{\mathbf{P}}^{\mathbf{C}} d\mathbf{s} \cdot \nabla_s \mathbf{V}(\mathbf{s}) + \boldsymbol{\Omega}_{PAC} \times (\mathbf{P} - \mathbf{C}) = [\boldsymbol{\Omega}_W(\mathbf{C}) - \boldsymbol{\Omega}_{PAC}] \times \mathbf{C} \quad (4)$$

and

$$\mathbf{V}(\mathbf{s}) = \boldsymbol{\Omega}_E(\mathbf{s}) \times \mathbf{s} \quad \boldsymbol{\Omega}_E(\mathbf{N}) = \boldsymbol{\Omega}_{NAM} \quad \text{along} \quad \text{CN}$$

$$\mathbf{V}(\mathbf{s}) = \boldsymbol{\Omega}_W(\mathbf{s}) \times \mathbf{s} \quad \boldsymbol{\Omega}_W(\mathbf{P}) = \boldsymbol{\Omega}_{PAC} \quad \text{along} \quad \text{CP}$$

Here, $\boldsymbol{\Omega}_{PAC}$ and $\boldsymbol{\Omega}_{NAM}$ are Euler poles for the rigid portions of the Pacific and North American plates. Between these rigid plates, deformation poles $\boldsymbol{\Omega}_E(\mathbf{s})$ and $\boldsymbol{\Omega}_W(\mathbf{s})$ describe motions of points s, east and west of the San Andreas. These poles, like all the vectors in this paper, are expressed in an arbitrary reference frame fixed at the center of the Earth. The difference between $\mathbf{V}_{PN}(\mathbf{C})$, the total Pacific-North America motion at C, and $\mathbf{V}_{SA}(\mathbf{C})$, the slip vector across the San Andreas fault at C, is termed the "San Andreas Discrepancy". The discrepancy is accounted for by $\mathbf{V}_E(\mathbf{C})$ and $\mathbf{V}_W(\mathbf{C})$, the path-integrated deformation along CN and CP.

Taking a $\mathbf{V}_{PN}(\mathbf{C})$ of 55.9±2.7 mm/yr (N35.5°±1.9°W) from global plate model RM2 [*Minster and Jordan*, 1978] and a $\mathbf{V}_{SA}(\mathbf{C})$ of 34±3 mm/yr (N41°±2°W) estimated from local geodetic networks [*Savage and Buford*, 1973; *Thatcher*, 1979; *Prescott et al.*, 1981] and Holocene geology [*Sieh and Jahns*, 1984], *Minster and Jordan* [1984] attempted to determine $\mathbf{V}_E(\mathbf{C})$, and indirectly $\mathbf{V}_W(\mathbf{C})$, by placing a variety of geological bounds [*Thompson and Burke*, 1973; *Wallace*,

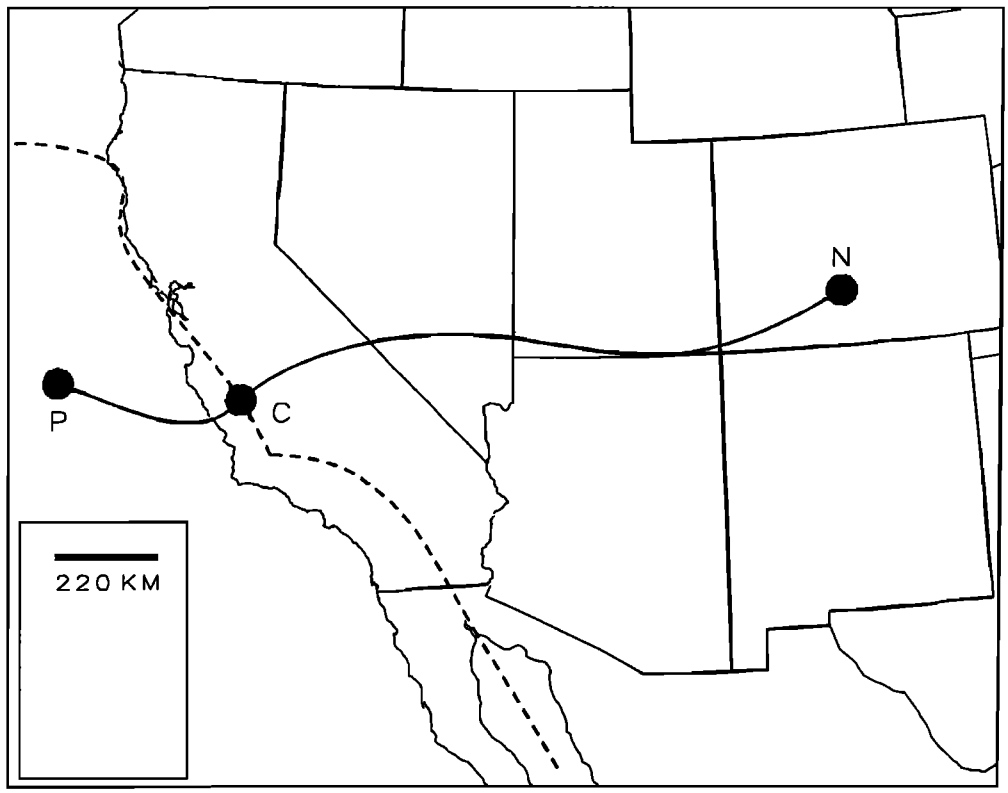

Fig. 2. Expanded view of the Pacific-North American margin showing the San Andreas fault (dashed line) and path NP between two points in the stable plate interiors.

1978; *Greensfelder et al.*, 1980; *Zoback and Zoback*, 1980] on $\Omega_E(s)$. The deformation pole for points along CN was found in a nonlinear, two-part procedure (direction first, then length) under the assumptions that $\Omega_E(s)$ is a polar field [$\Omega_E(s) = \omega(s)\hat{\Omega}_E$] and $\omega(s)$ is of a form such that there is no distributed shear across great circles containing $\pm\hat{\Omega}_E$. With the best geologically constrained $\mathbf{V}_E(C)$ (1-12 mm/yr, N65°±5°W) being too small and in the wrong direction to account for the discrepancy, they concluded that there must be substantial deformation along on the path CP.

Minster and Jordan [1987] later revised $\mathbf{V}_E(C)$ by incorporating eight VLBI-determined rates of baseline length change with the geological data into the bounds on $\Omega_E(C)$. Three models of $\mathbf{V}_E(C)$ were produced (A, 8.0±3.3 mm/yr (N64°±10°), purely geological; B, 9.0±3.9 mm/yr (N48°±17°), purely geodetic; C, 9.7±2.1 mm/y (N56°±10°), geological-geodetic) by varying the relative importance of the geological and geodetic constraints. All three of the newer models still required significant deformation west of C to account for the discrepancy.

With the current state of the VLBI network, it is now feasible to estimate all four terms in equation (1) directly from a linear inversion of VLBI-determined vector site velocities. This can be done for several points along the San Andreas without reference to a global plate model, geological and local geodetic measurements, or restrictions on distributed shear deformation.

Reduction to Vector Site Velocities

Reduction of the baseline data to a set of vector site velocities is straightforward [*Ward*, 1988]. Local north [$v_i^n\hat{\mathbf{n}}_i$, $v_j^n\hat{\mathbf{n}}_j$] and local east [$v_i^e\hat{\mathbf{e}}_i$, $v_j^e\hat{\mathbf{e}}_j$] velocities of VLBI sites at $\mathbf{P}_i$ and $\mathbf{P}_j$ are linked to the baseline B_{ij} and transverse T_{ij} rates in Table 1 by

$$\underset{(226\times 1)}{\begin{bmatrix} B_{ij} \\ T_{ij} \\ \vdots \end{bmatrix}} = \underset{(226\times 54)}{\begin{bmatrix} -\hat{\mathbf{b}}_{ij}\cdot\hat{\mathbf{n}}_i & -\hat{\mathbf{b}}_{ij}\cdot\hat{\mathbf{e}}_i & \hat{\mathbf{b}}_{ij}\cdot\hat{\mathbf{n}}_j & \hat{\mathbf{b}}_{ij}\cdot\hat{\mathbf{e}}_j \\ -\hat{\mathbf{t}}_{ij}\cdot\hat{\mathbf{n}}_i & -\hat{\mathbf{t}}_{ij}\cdot\hat{\mathbf{e}}_i & \hat{\mathbf{t}}_{ij}\cdot\hat{\mathbf{n}}_j & \hat{\mathbf{t}}_{ij}\cdot\hat{\mathbf{e}}_j \\ \vdots & \vdots & \vdots & \vdots \end{bmatrix}} \underset{(54\times 1)}{\begin{bmatrix} v_i^n \\ v_i^e \\ v_j^n \\ v_j^e \\ \vdots \end{bmatrix}} \tag{5}$$

where

$$\hat{\mathbf{b}}_{ij} = (\mathbf{P}_j - \mathbf{P}_i)/\,|\,\mathbf{P}_j - \mathbf{P}_i\,|$$

and

$$\hat{\mathbf{t}}_{ij} = \mathbf{P}_i\times\mathbf{P}_j/\,|\,\mathbf{P}_i\times\mathbf{P}_j\,|$$

Unless all of the stations are on the same great circle, equations (5) are full rank, and no further constraints are required to perform a weighted least squares inversion for the 54 velocity components v_i^n, v_i^e and their uncertainties $\mathrm{Cov}[v_i^n, v_i^e]$. The self-consistency of the VLBI measurements and the lack of significant vertical motion of the stations is apparent in the fact that the 54 velocities account for 99.4% of the variance in the 226 baseline data.

Rotation Poles From Vector Site Velocities

This paper devises several rigid plate tectonic models by fitting M groups of vector site velocities with equations of the form

$$\mathbf{V}_v(\mathbf{P}_i^q) = \underset{(2m_q \times 1)}{\begin{bmatrix} v_i^n \\ v_i^e \\ \vdots \end{bmatrix}} = \underset{(2m_q \times 1)}{\begin{bmatrix} \hat{\mathbf{n}}_i^q \cdot [\boldsymbol{\Omega}_q \times \mathbf{P}_i^q] \\ \hat{\mathbf{e}}_i^q \cdot [\boldsymbol{\Omega}_q \times \mathbf{P}_i^q] \\ \vdots \end{bmatrix}} =$$

$$\underset{(2m_q \times 3)}{\begin{bmatrix} (\mathbf{P}_i^q \times \hat{\mathbf{n}}_i^q)_x & (\mathbf{P}_i^q \times \hat{\mathbf{n}}_i^q)_y & (\mathbf{P}_i^q \times \hat{\mathbf{n}}_i^q)_z \\ (\mathbf{P}_i^q \times \hat{\mathbf{e}}_i^q)_x & (\mathbf{P}_i^q \times \hat{\mathbf{e}}_i^q)_y & (\mathbf{P}_i^q \times \hat{\mathbf{e}}_i^q)_z \\ \vdots & \vdots & \vdots \end{bmatrix}} \underset{(3 \times 1)}{\begin{bmatrix} (\Omega_q)_x \\ (\Omega_q)_y \\ (\Omega_q)_z \end{bmatrix}} \tag{6}$$

The $\boldsymbol{\Omega}_q$ ($q = 1, M$) are Euler poles, constant over the $m_q \geq 2$ VLBI sites assigned to the qth plate. Inverting vector site velocities to obtain $\boldsymbol{\Omega}_q$ has several advantages over an approach which substitutes (6) into (5) and estimates Euler poles directly from B_{ij} and T_{ij}:

1. Inversion (6) employs all of the information that VLBI supplies in Table 1, yet retains full flexibility to examine the behavior of subgroups of VLBI stations. This is crucial in quantifying plate stability.

2. Inversion (6) need not force a rigid plate assumption onto stations where the axiom is clearly violated, nor does it bias the Euler poles of rigid plate sites because of failures of the axiom elsewhere.

3. A χ^2 merit function for plate models can be formulated for just those stations where the rigid plate assumption has been validated.

4. Inconsistencies of 27 observed and predicted velocity vectors are easier to illustrate and interpret than are inconsistencies in 226 baseline and transverse rates.

Note that the velocities found in (5) and consequently, the plate rotation poles found from (6), are reference frame dependent in the sense that they derive from the specific set of transverse rates given in the GLB511 solution (D. Gordon, NASA GSFC) of Table 1. Because transverse rates are always uncertain within a rigid body rotation of the entire network, an arbitrary constant vector $\boldsymbol{\Omega}_R$ can be subtracted from all of the individual $\boldsymbol{\Omega}_q$ and a rotation $\boldsymbol{\Omega}_R \times \mathbf{P}_i^q$ can be subtracted from all velocities $\mathbf{V}_v(\mathbf{P}_i^q)$ without violating VLBI observations. Any choice of $\boldsymbol{\Omega}_R$ cancels out in vectors (1)-(4), however, and tectonic interpretations based on them can be considered frame independent. For the purpose of tabulating or illustrating frame dependent spatial fields after inversion (6), I prefer to let $\boldsymbol{\Omega}_R$ fix a reference plate and refer to observed and predicted vector velocities relative to it as

$$\mathbf{V}_o(\mathbf{P}_i^q) = \mathbf{V}_v(\mathbf{P}_i^q) - \begin{bmatrix} \hat{\mathbf{n}}_i^q \cdot [\boldsymbol{\Omega}_R \times \mathbf{P}_i^q] \\ \hat{\mathbf{e}}_i^q \cdot [\boldsymbol{\Omega}_R \times \mathbf{P}_i^q] \\ \vdots \end{bmatrix} \tag{7}$$

and

$$\mathbf{V}_p(\mathbf{P}_i^q) = \begin{bmatrix} \hat{\mathbf{n}}_i^q \cdot [\{\boldsymbol{\Omega}_q - \boldsymbol{\Omega}_R\} \times \mathbf{P}_i^q] \\ \hat{\mathbf{e}}_i^q \cdot [\{\boldsymbol{\Omega}_q - \boldsymbol{\Omega}_R\} \times \mathbf{P}_i^q] \\ \vdots \end{bmatrix} \tag{8}$$

Figure 3 maps and Table 3 lists $\mathbf{V}_o(\mathbf{P}_i^q)$ where $\boldsymbol{\Omega}_R$ is selected to minimize the velocities of six interior North America stations. This choice is representative of a "fixed central North America" frame and returns site velocities similar to those found by other workers who employ an analogous reference [*Clark et al.*, 1987; *Gordon and Sauber*, 1988].

Four VLBI Plate Motion Models

To address the questions proposed in the introduction, I construct four VLBI-based plate models, designated: VM1A, VM1B, VM2, and VM3. Construction of plate models is an important advancement beyond free-site inversions (5) and Figure 3. By determining the Euler poles of a few plates upon which several stations ride, bias and errors in the velocities of individual sites can be averaged out and failures of the rigid plate assumption will be easy to document. In addition, this approach makes it possible to quantify the consistency of specified plate models against the VLBI data set as a whole, and not just individual baseline rates or site vectors [*Gordon et al.*, 1988].

The VM models contain as many as six Euler poles derived from equation (6) in two independent steps. Step I finds $\boldsymbol{\Omega}_{NAM}$, $\boldsymbol{\Omega}_{PAC}$ and tests the observed Pacific-North America velocities against RM2 and NUVEL 1 [*DeMets et al.*, 1990] predictions. Step I also tests the necessity of deformation west along CP. Step II investigates how path integrated deformation is partitioned in the borderland to the east of C. To best perform its tests, Step I employs vector site velocities from just the ten stations thought to be attached to the stable interiors of the North America (Ft. Davis, Yuma, Flagstaff, Platteville, Westford, and Fairbanks) and Pacific plates (Vandenberg, Ft. Ord, Kwajalein, and Kauai). The consistency of a rigid plate assumption and the observed vector velocities of these ten sites is examined after the fact.

Step I. VM1A and VM1B are reference models where the Pacific-North America pole is fixed at the RM2 and NUVEL 1 values, respectively, and the four Pacific sites are placed on a single plate. In VM2 and VM3 the Pacific-North America pole is freed. Furthermore, in VM3, relative motion between the central Pacific (Kwajalein and Kauai) and eastern Pacific (Vandenberg and Ft. Ord) is permitted through the introduction of a Vandenberg plate (Figure 4) with pole $\boldsymbol{\Omega}_{VND}$. VM3 supplies Pacific-North America motion without assuming that the California coastal sites are firmly attached to a rigid Pacific plate. Also, by admitting an articulated plate, VM3 can distinguish $\boldsymbol{\Omega}_W(\mathbf{C})$. A merit function

$$\chi^2 = \sum_{i=1}^{10} \delta\mathbf{V}^T(\mathbf{P}_i)\mathrm{Cov}^{-1}[v_i^n, v_i^e]\delta\mathbf{V}(\mathbf{P}_i)$$

$$\delta\mathbf{V}(\mathbf{P}_i) = [\mathbf{V}_o(\mathbf{P}_i) - \mathbf{V}_p(\mathbf{P}_i)] \tag{9}$$

derived from the weighted residuals of local north and east velocities at the 10 interior sites forms the basis for statistical tests.

Step II. After ascertaining $\boldsymbol{\Omega}_{NAM}$, $\boldsymbol{\Omega}_{PAC}$, and $\boldsymbol{\Omega}_{VND}$ in step I, the vector velocities of the sixteen remaining sites are introduced into (6) to obtain $\boldsymbol{\Omega}_{BLN}$, $\boldsymbol{\Omega}_{NCA}$, and $\boldsymbol{\Omega}_{SCA}$, the Euler poles of three hypothetical plates in the deforming borderland (Figure 4). In this way, integrated deformation vectors $\mathbf{V}_W$ and $\mathbf{V}_E$ can be found along three paths NP through points C (36.0°N, 120.6°W), D (34.1°N, 117.0°W), and E (39.0°N, 123.9°W) in central, southern, and northern California. Generally, plate boundaries within the borderland coincide with geological provinces and major faults. Neither the detailed partitioning nor the consistency of a rigid plate assumption within the borderland are particularly important however, because only path integrated deformation is desired, not a specific spatial distribution.

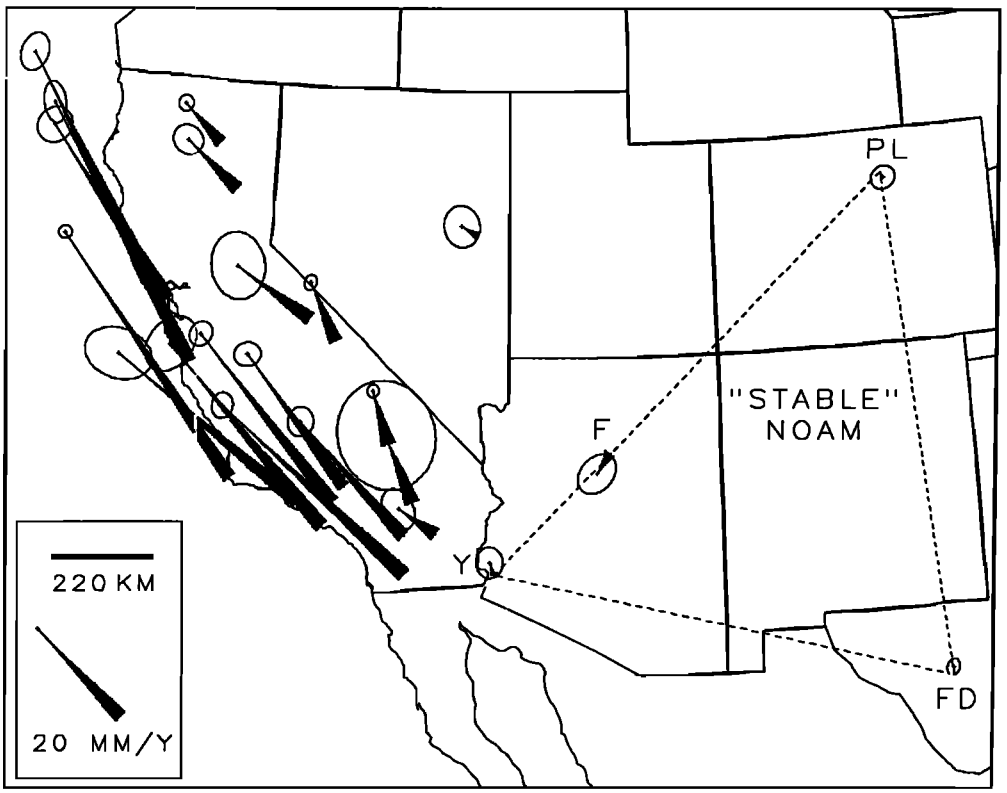

Fig. 3. Observed site velocities $\mathbf{V}_o(\mathbf{P}_i)$ for western North America and their 3σ error ellipses. Lengths of the vectors can be compared with the 20 mm/yr standard vector in the box to determine site speeds. The observation frame minimizes the velocities of six interior sites on the North America plate: Ft. Davis (FD), Flagstaff (F), Platteville (PL), Yuma (Y), Westford, and Fairbanks. The stable portion of North America is reached somewhere near the Colorado Plateau.

TABLE 3. Observed $\mathbf{V}_o(\mathbf{P}_i)$ Site Velocities, Azimuths, and Related Uncertainties

Site	Velocity, mm/yr	Azimuth, deg	σ_1, mm/yr	θ_1, deg	σ_2, mm/yr	θ_2, deg
FAIRBNKS	2.6	203.7	0.8	44	0.6	134
HATCREEK	8.5	312.4	0.4	165	0.4	75
KASHIMA	3.6	311.1	1.3	149	1.2	59
KAUAI	77.1	316.0	1.0	138	0.9	48
KWAJLEIN	75.9	306.6	1.8	23	1.7	113
MOJAVE	9.0	340.4	0.4	8	0.3	98
VNDNBERG	48.1	321.3	0.4	93	0.4	3
BLKBUTTE	7.5	302.1	1.2	149	0.8	59
DEADMANL	11.7	335.9	3.0	153	2.7	63
ELY	3.1	297.5	1.1	165	1.0	75
FLAGSTAF	4.1	213.7	1.2	43	0.9	133
FT.DAVIS	1.3	359.2	0.5	21	0.3	111
FT.ORD	47.4	326.8	1.1	166	0.6	76
JPL	34.8	318.5	0.7	36	0.6	126
MAMMOTHL	14.6	302.3	1.8	167	1.5	77
MONPEAK	40.8	310.5	0.7	12	0.6	102
OVRO	10.4	332.9	0.4	17	0.3	107
PBLOSSOM	26.7	320.4	0.7	77	0.6	167
PINFLATS	25.4	315.3	0.8	8	0.7	98
PLATTVIL	1.0	156.7	0.7	55	0.6	145
PT.REYES	41.4	326.8	1.0	16	0.7	106
PRESIDIO	33.7	320.8	1.0	51	0.9	141
PVERDES	38.6	316.8	1.7	39	1.2	129
QUINCY	11.4	309.4	0.9	121	0.8	31
SANPAULA	38.1	305.5	1.9	105	1.3	15
WESTFORD	3.8	163.0	0.9	179	0.5	89
YUMA	2.2	338.1	0.8	173	0.7	83

The observation frame minimizes the velocities of the six interior North American sites. σ_i and θ_i are the length and orientation of the semimajor axes of the one σ velocity error ellipse.

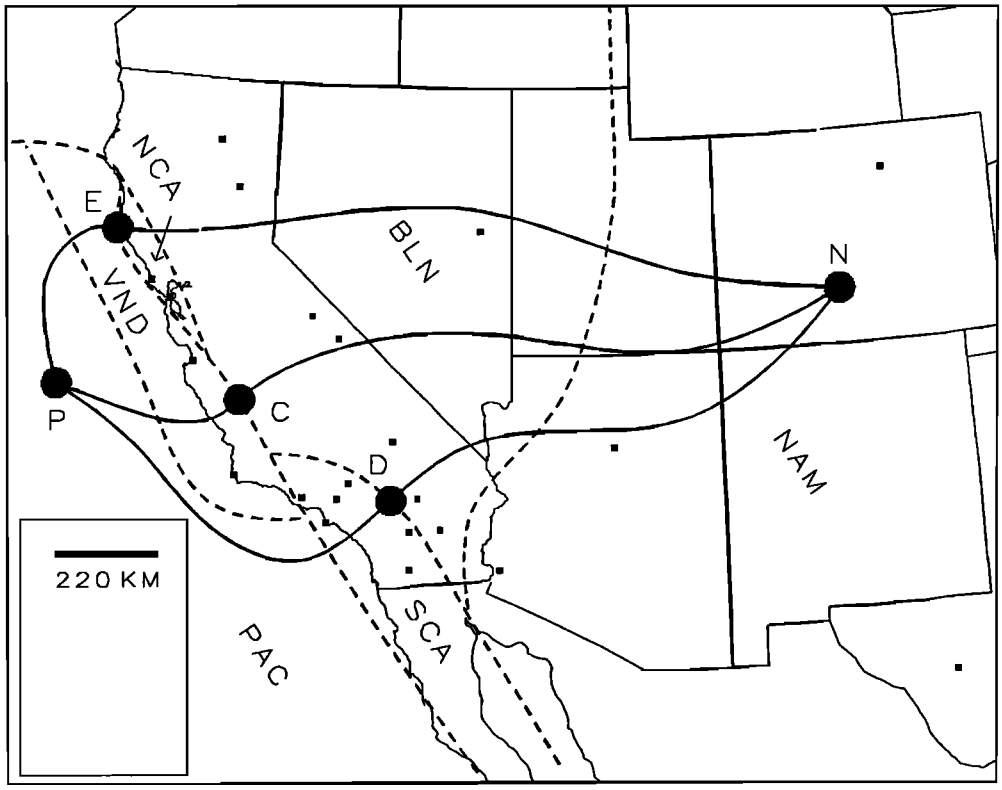

Fig. 4. Map illustrating the six plates (North America (NAM), Borderland (BLN), Northern California (NCA), Southern California (SCA), Vandenberg (VND), Pacific (PAC)) contained in the VM models. The North America plate contains the six stations: Ft. Davis, Plattville, Flagstaff, Yuma, Westford, and Fairbanks. The Pacific plate contains the four sites: Vandenberg, Ft. Ord, Kwajalein, and Kauai. In VM3, Vandenberg and Ft. Ord are detached onto the Vandenberg plate to test the need for offshore deformation in central California. Euler poles of the Borderland, Northern California, and Southern California plates are used to estimate path integrated deformation along NC, ND, and NE.

The Borderland plate encompasses the Basin and Range westward from the Wasatch Front, the Sierra Nevada Block, and the Great Valley to the central San Andreas and contains eight VLBI sites (Ely, Hatcreek, Quincy, Owens Valley, Mammoth Lakes, Black Butte, Mojave, and Deadman Lake). The Northern California plate is bounded at the coast by the San Andreas and inland by the Calaveras, Hayward, and the Rogers Creek-Healdsberg faults extended northward to Cape Mendocino. The Presidio and Pt. Reyes stations are on the Northern California plate. The Southern California plate is bounded on the east by the San Andreas south of the big bend and on the west at the Channel Islands by an extension of a small circle formed by the central San Andreas. The Southern California plate contains six VLBI sites (Jet Propulsion Laboratory, Pearblossom, Pinyon Flats, Palos Verdes, Santa Paula, and Monument Peak).

Deformation poles in the VM models at **C**, **D**, and **E** reduce to

$$\begin{aligned} \boldsymbol{\Omega}_E(\mathbf{C}) &= \boldsymbol{\Omega}_E(\mathbf{D}) = \boldsymbol{\Omega}_{BLN} \\ \boldsymbol{\Omega}_E(\mathbf{E}) &= \boldsymbol{\Omega}_{NCA} \\ \boldsymbol{\Omega}_W(\mathbf{D}) &= \boldsymbol{\Omega}_{SCA} \\ \boldsymbol{\Omega}_W(\mathbf{C}) = \boldsymbol{\Omega}_W(\mathbf{E}) &= \begin{matrix} \mathbf{0} & VM1, VM2 \\ \boldsymbol{\Omega}_{VND} & VM3 \end{matrix} \end{aligned} \tag{10}$$

Note from Figure 4 that $\mathbf{V}_E(\mathbf{E})$ has two parts, accumulated motion across the Borderland plate, $\mathbf{V}_E^1(\mathbf{E})$, and slip near the northern California-Borderland boundary, $\mathbf{V}_E^2(\mathbf{E})$. VLBI-determined San Andreas slip vectors are found from (1)-(4) and (10) through

$$\begin{aligned} \mathbf{V}_{SA}(\mathbf{D}) &= [\boldsymbol{\Omega}_{SCA} - \boldsymbol{\Omega}_{BLN}] \times \mathbf{D} \\ \mathbf{V}_{SA}(\mathbf{C}) &= \begin{matrix} [\boldsymbol{\Omega}_{PAC} - \boldsymbol{\Omega}_{BLN}] \times \mathbf{C} & VM1, VM2 \\ [\boldsymbol{\Omega}_{VND} - \boldsymbol{\Omega}_{BLN}] \times \mathbf{C} & VM3 \end{matrix} \\ \mathbf{V}_{SA}(\mathbf{E}) &= \begin{matrix} [\boldsymbol{\Omega}_{PAC} - \boldsymbol{\Omega}_{NCA}] \times \mathbf{E} & VM1, VM2 \\ [\boldsymbol{\Omega}_{VND} - \boldsymbol{\Omega}_{NCA}] \times \mathbf{E} & VM3 \end{matrix} \end{aligned} \tag{11}$$

Tables 4-9 summarize predicted and observed site velocities, statistics, relative motion vectors, and Euler poles of the VM models. Figures 5, 8 and 10 plot $\mathbf{V}_{PN}, \mathbf{V}_{SA}, \mathbf{V}_W$ $\mathbf{V}_E$, and their 3σ error ellipses on the tangent plane at the three fiducial points.

Of the 55.8 mm/yr (N36°W) of Pacific-North America motion at **C** in reference model VM1A, 12.6±1.0 mm/yr (N31°±4°W) is absorbed across the Borderland while the remainder, 43.2±1.0 mm/yr (N37°±1°W) is accommodated by slip at the San Andreas. Figure 6 plots the best fitting site velocities with VM1A predictions for the 10 interior stations. It is obvious, even by eye, that RM2 does not fit VLBI data very well. VM1A has a χ^2 variance of 523.

TABLE 4. Observed $\mathbf{V}_o(\mathbf{P}_i)$ and Predicted $\mathbf{V}_p(\mathbf{P}_i)$ Site Velocities and Directions of the VM Models

Site	Observed		VM1A Predicted		VM1B Predicted		VM2 Predicted		VM3 Predicted	
	Velocity mm/yr	Azimuth deg	Velocity mm/yr	Azimuth deg	Velocity mm/y	Azimuth deg	Velocity mm/y	Azimuth deg	Velocity mm/y	Azimuth deg
FAIRBNKS	2.6	203.7	6.6	185.6	1.9	202.5	0.0	-	0.0	-
KAUAI	77.1	316.0	80.3	313.2	78.3	314.4	76.1	314.1	77.1	316.0
KWAJLEIN	75.6	306.9	82.7	304.9	83.1	306.9	79.8	306.3	76.0	306.4
VNDNBERG	48.1	321.3	52.5	322.1	48.1	322.2	47.8	322.4	48.0	321.7
FLAGSTAF	4.1	213.7	3.4	149.2	0.5	146.9	0.0	-	0.0	-
FT.DAVIS	1.3	359.2	3.1	129.5	0.5	97.0	0.0	-	0.0	-
FT.ORD	47.4	326.8	51.9	324.3	47.5	324.8	47.2	324.9	47.2	325.5
PLATTVIL	1.0	156.7	2.2	161.6	0.1	202.8	0.0	-	0.0	-
WESTFORD	3.8	163.0	2.4	7.4	1.3	2.8	0.0	-	0.0	-
YUMA	2.2	338.1	4.0	145.7	0.6	142.1	0.0	-	0.0	-

The observation frame minimizes the velocities of the six interior North American sites.

TABLE 5. Summary of VLBI Plate Model Statistics

Model	Permitted Rotations	Number of Parameters	DOF	χ^2	Significance of Improvement, %
VM1A	Ω_{NAM}	3	17	523.4	-
VM1B	Ω_{NAM}	3	17	111.1	99
VM2	$\Omega_{NAM}, \Omega_{PAC}$	6	14	90.9	99/50
VM3	$\Omega_{NAM}, \Omega_{PAC}, \Omega_{VND}$	9	11	66.2	99/54/54

Chi-square is based on the fit to 20 data, the local north and local east velocity of the ten interior sites (equation 9). First, second and third numbers in the right column refer to the improvement over VM1A, VM1B, and VM2.

TABLE 6. Summary of Relative Plate Velocities at Point C, 36.0°N, 120.6°W

Model	$\mathbf{V}_{PN}$	$\mathbf{V}_{SA}$	$\mathbf{V}_E$	$\mathbf{V}_W$
VM1A (RM2)	55.8 N36°W	43.2±1.0 N37°±1°W	12.6±1.0 N31°±4°W	
VM1B (NUVEL)	47.8 N36°W	38.8±1.0 N36°±1°W	9.0±1.0 N33°±6°W	
VM2	46.8±1.4 N36°±2°W	38.6±1.3 N36°±2°W	8.2±1.3 N34°±7°W	
VM3	52.1±7.3 N31°±4°W	38.3±1.3 N36°±2°W	8.2±1.3 N34°±7°W	7.2±7.3 N6°±37°E

In VM1A and VM1B, $\mathbf{V}_{PN}$ is constrained to the RM2 and NUVEL 1 values. Uncertainties are 3σ. Velocities are in mm/yr.

TABLE 7. Summary of Relative Plate Velocities at Point D, 34.1°N, 117.0°W

Model	$\mathbf{V}_{PN}$	$\mathbf{V}_{SA}$	$\mathbf{V}_E$	$\mathbf{V}_W$
VM1A (RM2)	54.2 N38°W	25.0±1.1 N52°±3°W	12.9±0.9 N27°±5°W	17.7±1.1 N26°±4°W
VM1B (NUVEL)	46.3 N39°W	25.0±1.1 N52°±3°W	9.4±0.9 N26°±7°W	13.4±1.2 N23°±5°W
VM2	45.4±1.4 N39°±2°W	25.0±1.1 N52°±3°W	8.8±1.1 N25°±8°W	13.3±1.6 N21°±5°W
VM3	50.5±7.3 N32°±5°W	25.0±1.1 N52°±3°W	8.8±1.1 N25°±8°W	19.8±8.0 N10°±8.0°W

In VM1A and VM1B, $\mathbf{V}_{PN}$ is constrained to the RM2 and NUVEL 1 values. Uncertainties are 3σ. Velocities are in mm/yr.

VM1B, the NUVEL 1 based reference model, reproduces VLBI data far better than RM2. NUVEL 1 cuts Pacific-North America motion to 47.8 mm/yr, but still overpredicts velocities at the two western Pacific sites (Figure 7 and Table 4). A standard F-test indicates that the χ^2 reduction of VM1B over VM1A (111 versus 523) is significant at the 99% confidence level (Table 5).

When unconstrained in VM2, Pacific-North America rates drop still further (Figure 8). Of the 46.8±1.4 mm/yr (N36°±2°W) of motion at C, the Borderland and the San Andreas now absorb 8.2±1.3 mm/yr (N34°±7°W) and 38.6±1.3 mm/yr (N36°±2°W). The VM2 Pacific-North America pole lies midway between the RM2 and NUVEL 1 poles and contains them both within 3σ error bounds (Figure 9). Mean Pacific-North America velocities at points C, D, and E in RM2 and NUVEL 1 are 19% and 2% more then VM2, respectively. The χ^2 reduction of VM2 with respect to RM2 and NUVEL 1 (91 versus 523 and 111) is significant at the 99% and 50% levels.

Detaching the central coast of California from the Pacific plate in VM3 further cuts χ^2 error at the expense of enlarged uncertainties in $\mathbf{V}_{PN}$. Total motion increases at C to 52.1±7.3 mm/yr (N31°±4°W) with the introduction of a barely resolvable offshore component of Pacific plate deformation, $\mathbf{V}_W(\mathbf{C}) = 7.2\pm7.3$ mm/yr (N6° ± 37°E) (see Figures 10 and 11). Compared with VM1A and VM2 the χ^2 reduction of VM3 (66 versus 523 and 91) is significant at the 99% and 54% levels. In its current state, VLBI does not demand any deformation offshore central California. VLBI does indicate that there is a 93% likelyhood that Pacific-North America motion is less than RM2 predictions even if Vandenberg and Ft. Ord are not fully on the Pacific plate.

The statistical consistency of the VLBI plate models can

TABLE 8. Summary of Relative Plate Velocities at Point E, 39.0°N, 123.9°W

Model	$\mathbf{V}_{PN}$	$\mathbf{V}_{SA}$	$\mathbf{V}_E^1$	$\mathbf{V}_E^2$	$\mathbf{V}_W$
VM1A (RM2)	56.5 N32°W	14.9±2.0 N23°±8°W	12.6±1.1 N36°±6°W	29.3±2.0 N35°±4°W	
VM1B (NUVEL)	48.4 N32°W	10.9±2.1 N14°±10°W	8.9±1.0 N42°±8°W	29.3±2.0 N35°±4°W	
VM2	47.4±1.4 N32°±2°W	10.6±2.1 N14°±11°W	8.2±1.3 N46°±11°W	29.3±2.0 N35°±4°W	
VM3	52.9±7.3 N28°±3°W	11.5±2.6 N4°±16°W	8.2±1.3 N46°±11°W	29.3±2.0 N35°±4°W	5.6±7.0 N14°±55°W

In VM1A and VM1B, $\mathbf{V}_{PN}$ is constrained to the RM2 and NUVEL 1 values. Uncertainties are 3σ. Velocities are in mm/yr.

TABLE 9. Summary of Plate Rotation Poles Relative to North America

Model	$\Omega_{PAC} - \Omega_{NAM}$	$\Omega_{BLN} - \Omega_{NAM}$	$\Omega_{SCA} - \Omega_{NAM}$	$\Omega_{NCA} - \Omega_{NAM}$	$\Omega_{VND} - \Omega_{NAM}$
VM1A (RM2)	48.8°N 73.9°W 0.852°/Ma	0.8°±25.7°S 16.2°±25.5°E 0.142°±0.057°/Ma	52.1°±1.9°N 74.6°±10.1°W 0.579°±0.092°/Ma	31.5°±3.6°N 15.2°±4.0°W 0.379°±0.017°/Ma	
VM1B (NUVEL 1)	48.7°N 78.2°W 0.783°/Ma	17.2°±16.9°S 33.9°±17.1°E 0.165°±0.085°/Ma	53.1°±2.2°N 73.2°±14.4°W 0.513°±0.104°/Ma	26.1°±3.7°N 6.8°±4.0°W 0.344°±0.018°/Ma	
VM2	49.0°±0.9°N 75.2°±3.2°W 0.729°±0.035°/Ma	21.0°±15.0°S 38.9°±16.0°E 0.186°±0.109°/Ma	53.6°±2.2°N 71.1°±14.1°W 0.487°±0.098°/Ma	23.2°±4.8°N 2.8°±5.5°W 0.339°±0.017°/Ma	
VM3	45.6°±3.3°N 66.8°±10.4°W 0.714°±0.035°/Ma	21.0°±15.0°S 38.9°±16.0°E 0.186°±0.109°/Ma	53.6°±2.2°N 71.1°±14.1°W 0.487°±0.098°/Ma	23.2°±4.8°N 2.8°±5.5°W 0.339°±0.017°/Ma	47.4°±2.2°N 89.4°±13.9°W 0.966°±0.270°/Ma

In VM1A and VM1B, $\Omega_{PAC} - \Omega_{NAM}$ is constrained to the RM2 and NUVEL 1 values. Uncertainties are 3σ.

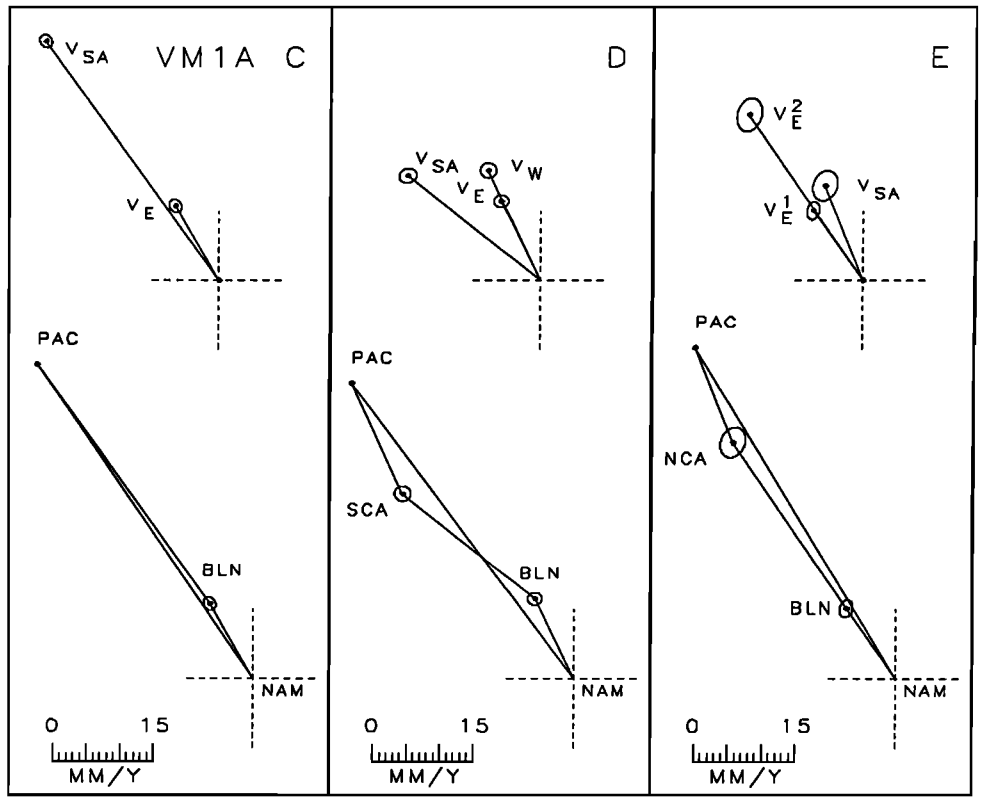

Fig. 5. (Top) Individual and (Bottom) summed plate motion vectors $\mathbf{V}_{PN}, \mathbf{V}_{SA}, \mathbf{V}_E$, and $\mathbf{V}_W$ for VM1A (RM2) projected on the tangent plane at points C, D, and E. Error ellipses are 3σ.

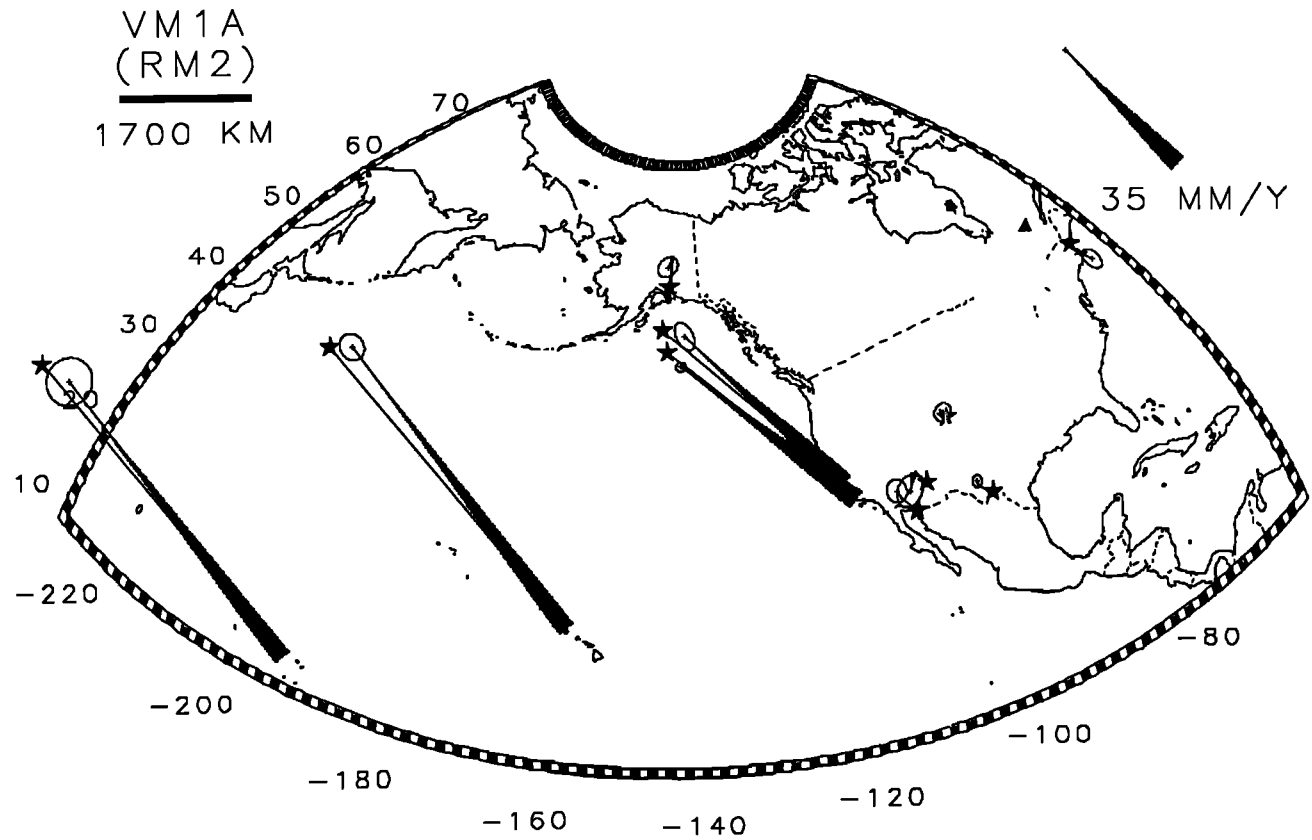

Fig. 6. Plots of observed $\mathbf{V}_o(\mathbf{P}_i)$ (solid arrows) and theoretical $\mathbf{V}_p(\mathbf{P}_i)$ (starred vectors) site velocities for VM1A (RM2) at the 10 interior sites. The triangle in eastern Canada is the RM2 Pacific-North America pole. RM2 plate rates are clearly inconsistent with VLBI observations. VM1A fits the velocities of the 10 interior sites within 5.5 σ.

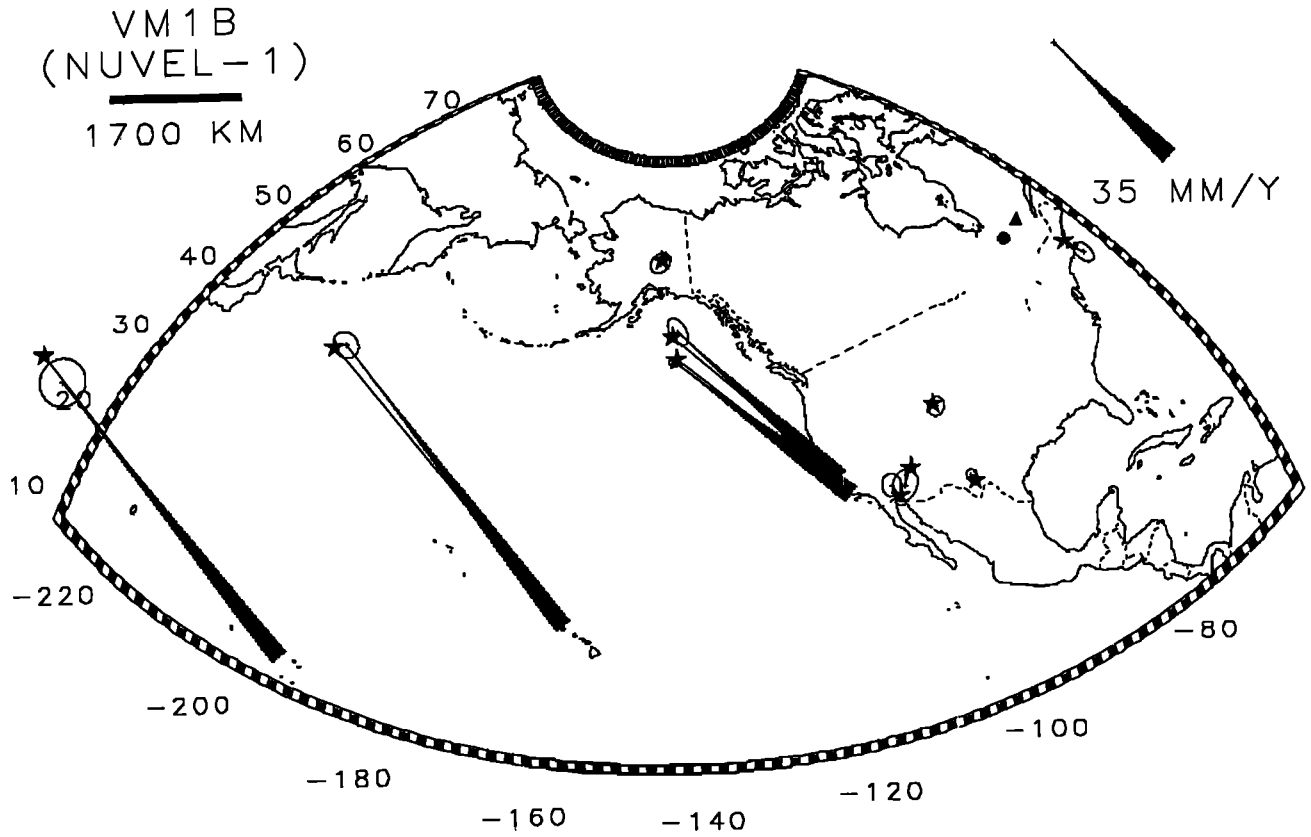

Fig. 7. Plots of observed $\mathbf{V}_o(\mathbf{P}_i)$ (solid arrows) and theoretical $\mathbf{V}_p(\mathbf{P}_i)$ (starred vectors) site velocities for VM1B (NUVEL 1) at the 10 interior sites. The triangle and circle in eastern Canada are the RM2 and NUVEL 1 Pacific-North America poles. NUVEL 1 significantly improves RM2's fit to VLBI data, although it still overpredicts velocities at the two western Pacific sites. VM1B fits the velocities of the 10 interior sites within 2.6 σ.

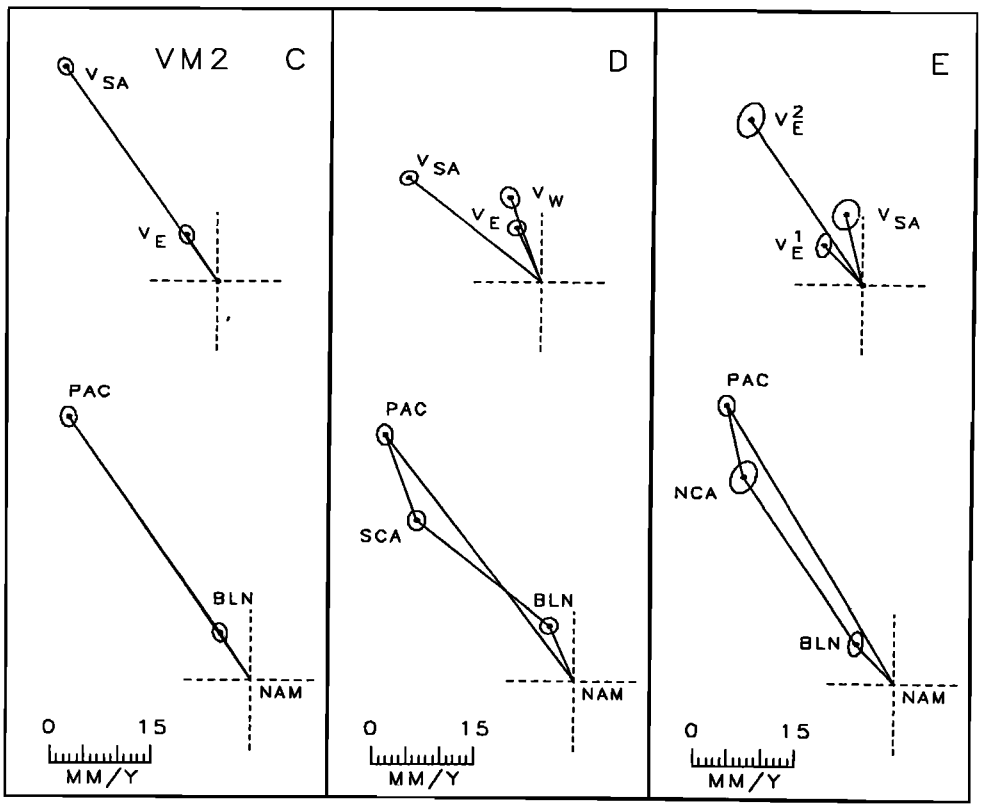

Fig. 8. (Top) Individual and (Bottom) summed plate motion vectors $\mathbf{V}_{PN}, \mathbf{V}_{SA}, \mathbf{V}_E$, and $\mathbf{V}_W$ for VM2 projected on the tangent plane at points C, D, and E. Error ellipses are 3σ.

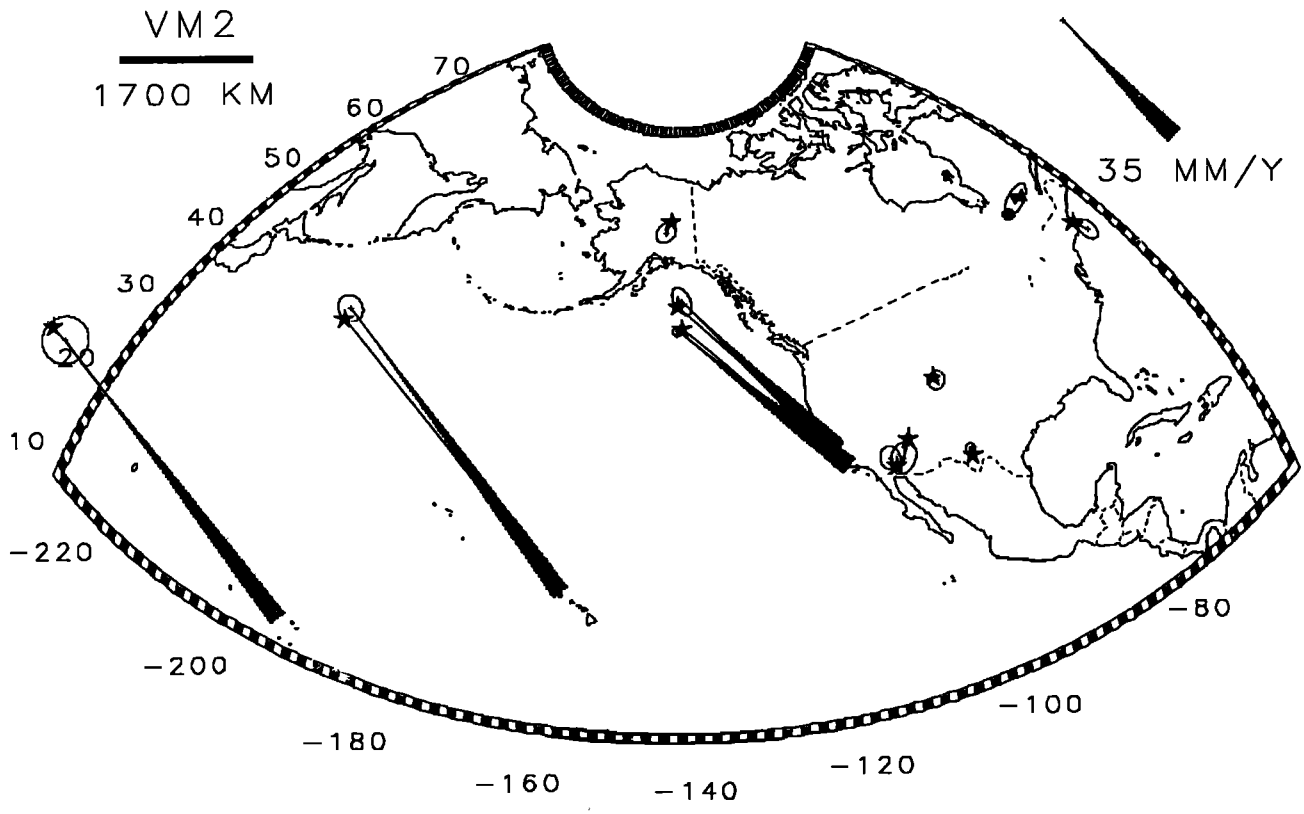

Fig. 9. Plots of observed $\mathbf{V}_o(\mathbf{P}_i)$ (solid arrows) and theoretical $\mathbf{V}_p(\mathbf{P}_i)$ (starred vectors) site velocities for VM2 at the 10 interior sites. VM2 corrects the systematic misfit of NUVEL 1 and fits the velocities of the 10 stable sites within 2.5 σ. The remaining error reflects the degree of consistency of VLBI data and the rigid plate assumption at the 10 sites. The triangle, circle, and inverted triangle in eastern Canada are the RM2, NUVEL 1, and VM2 Pacific-North America poles. All errors are 3σ.

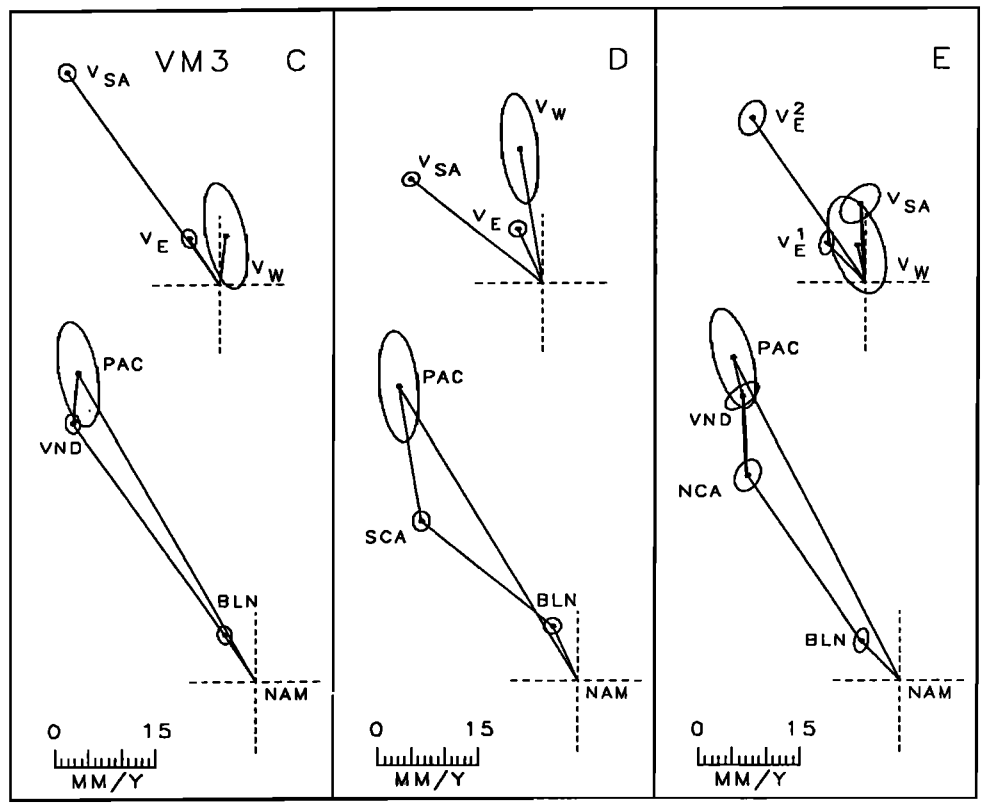

Fig. 10. (Top) Individual and (Bottom) summed plate motion vectors $\mathbf{V}_{PN}, \mathbf{V}_{SA}, \mathbf{V}_E$, and $\mathbf{V}_W$ for VM3 projected on the tangent plane at points C, D, and E. Error ellipses are 3σ.

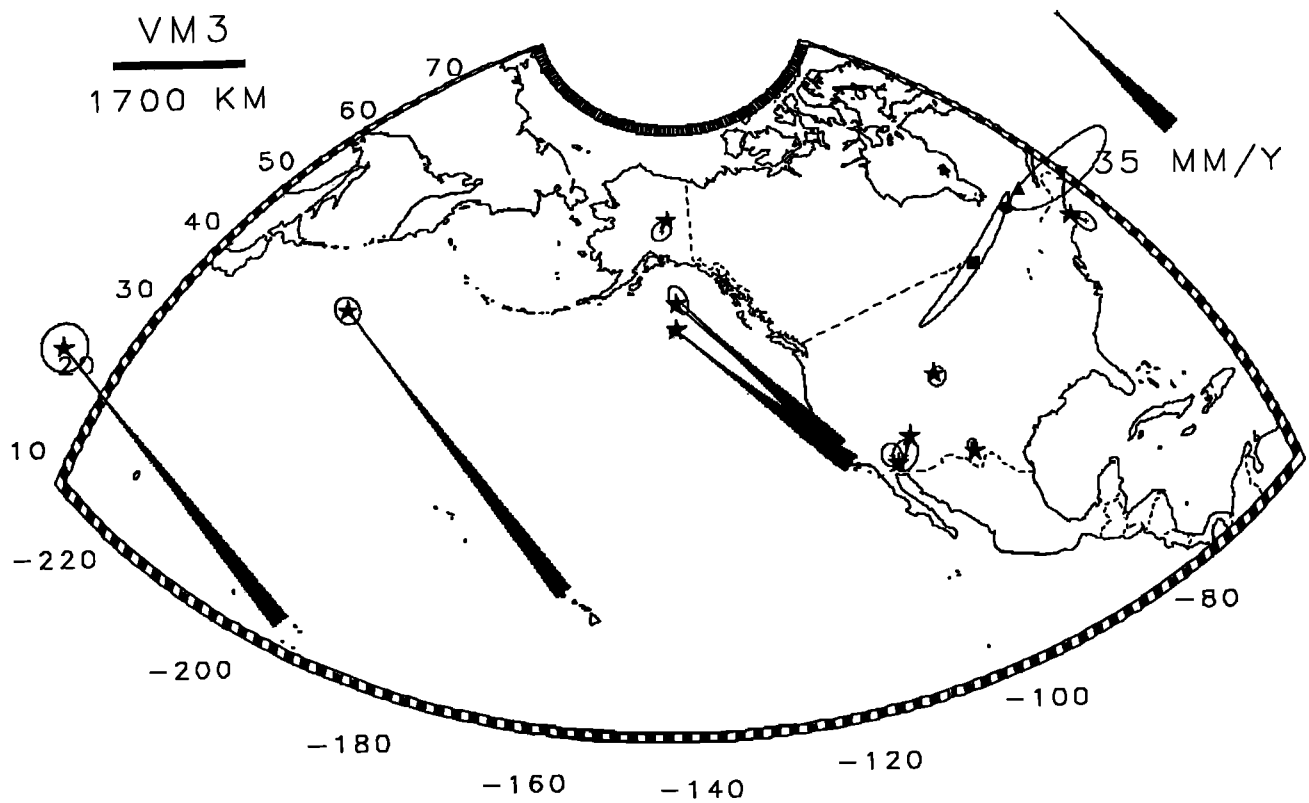

Fig. 11. Plots of observed $\mathbf{V}_o(\mathbf{P}_i)$ (solid arrows) and theoretical $\mathbf{V}_p(\mathbf{P}_i)$ (starred vectors) site velocities for VM3 at the ten interior sites. Breaking the Pacific into two plates provides a much better fit of Pacific site velocities at the expense of larger uncertainties in pole positions. The triangle, circle, and inverted triangle in eastern Canada are the RM2, NUVEL 1, VM2 and VM3 Pacific-North America poles. The square at the U.S-Canada border is the Vandenberg-North America pole. All errors are 3σ.

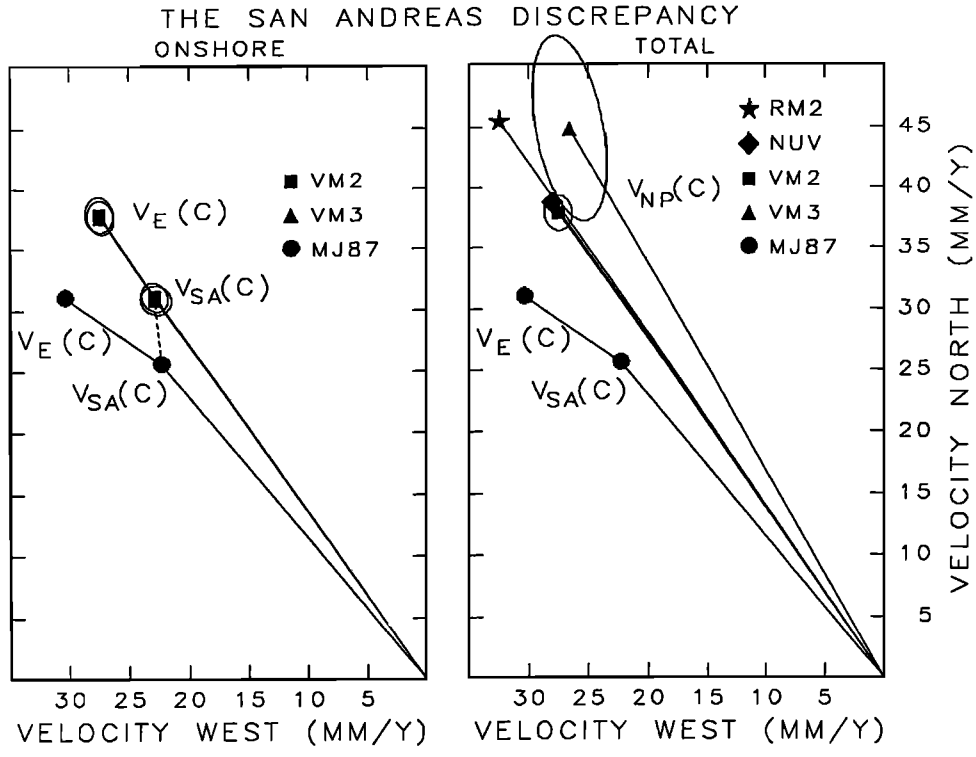

Fig. 12. (Left) Comparison of San Andreas slip $\mathbf{V}_{SA}$(C) and path integrated deformation $\mathbf{V}_E$(C) vectors from *Minster* and *Jordan's* [1987] model "C" and the VLBI models VM2 and VM3. Difference between the two $\mathbf{V}_{SA}$ (dashed line) probably represents onshore deformation west of the San Andreas. (Right) Plots of $\mathbf{V}_{SA}$, $\mathbf{V}_E$ from model "C" and $\mathbf{V}_{PN}$ from RM2, NUVEL 1, VM2, and VM3.

be examined using reduced chi-square, $\chi^2_R = \chi^2/$(number of degrees of freedom). χ^2_R greater than unity implies either that errors in the data have been underestimated or that the model is inadequate. VM1A, VM1B, VM2, and VM3 have χ^2_R of 30.8, 6.5, 6.5, and 6.0, respectively. Included in these numbers are two sources of misfit: mislocation of relative rotation poles and the failure of the underlying rigid plate assumption. It is useful to separate the two errors as their geophysical interpretations are very distinct. The first relates to plate tectonic modeling, while the second addresses questions of plate stability and the VLBI error budget.

Pacific and North America plate stability can be quantified by checking the consistency of vector site velocities with rigid plate motion. Taken separately, the velocities of the four interior Pacific and six interior North America VLBI sites are consistent with rigid one-plate motion at 2.4σ and 2.6σ. The nearly equal values of stability suggest a comparable degree of heterogeneity of mechanical properties and strain fields within the continental and oceanic lithospheres. Together, the vector velocities of the ten interior sites are consistent with rigid two-plate motion within 2.5σ ($2.5 = \sqrt{\chi^2_R}$ for VM2).

The excess χ^2_R for the 10 interior sites can be attributed to unrealistically small (by 2.5 times) estimates of VLBI errors, minor tectonic deformation within the assumed rigid plates, or both. Either way, when judging the consistency of plate tectonic models with χ^2 criteria, errors can be scaled to account for misfit due to plate stability. In this case, only errors greater than 2.5σ result solely from misplacement of relative rotation poles. If all the errors in Table 1 were uniformly increased by a factor of 2.5, reduced chi-square for VM1A, VM1B, VM2, and VM3 would be 4.7, 1.0, 1.0, and 0.9. RM2 is incompatible with VLBI measurements even after accounting for inconsistencies due to the plate stability. Based on errors due to pole positions alone, VM1B, VM2, and VM3 are equally consistent.

Tectonic Implications of VM2/3 at Point C: The San Andreas Discrepancy

V_{SA}. Instantaneous VLBI (38.6±1.3 mm/yr, N36°±2°W) and average Holocene (34±3 mm/yr, N41°±2°W) values of San Andreas slip differ by 5.6 mm/yr (N4°W) (*left*, Figure 12). Because VLBI lends little support for deformation of the Pacific plate offshore between Vandenberg-Ft. Ord and Kauai-Kwajalein, it is likely that the additional 4.4±1.3 and 3.4±1.0 mm/yr of motion parallel and normal to the San Andreas is accumulated onshore just west of C. Right-lateral shear and compression of this style are consistent with the integrated deformation (7±1 mm/yr, N03°±13°E) observed from geodetic networks spanning the Santa Maria Basin [*Feigl et al.*, 1990].

V_E. VM2's rate of Basin and Range spreading (8.2±1.3 mm/yr) is in good agreement with the geological value (8.0±3.3 mm/yr) established by *Minster and Jordan* [1987] in their model "A". The directions of spreading however, diverge by 30° with VM2 taking a more northerly heading (N34°±7°W versus N64°±10°W). It is unclear whether the azimuth discrepancy represents a contrast in geologic versus geodetic data or different analysis techniques. Interestingly,

the direction of $\mathbf{V}_E(\mathbf{C})$ in the *Minster and Jordan* [1987] models migrates toward the VM2 heading (N65°±10°W→ N56°±10°W → N48°±17°W) as geodetic constraints are made increasingly more important relative to geological constraints. The more westerly azimuth of $\mathbf{V}_E(\mathbf{C})$ in the Minster and Jordan models may also result from their assumption forbiding distributed shear across great circles containing $\pm\hat{\Omega}_E$. This restriction reduces Basin and Range deformation to pure uniaxial extension and confines $\hat{\Omega}_E$ to a direction perpendicular to the mean trend of observed principal extensional strain. Right-lateral strike slip on NNE trending Basin and Range faults is suppressed in these models and may force a more westerly direction of deformation.

V_W. VLBI does not demand any Pacific plate deformation offshore in central California. Of course, uncertainties in the motion of Kauai and Kwajalein are still large, and VM3 can not reject as much as 15 mm/yr of Pacific plate deformation at 3σ. If all the deformation was projected on northwest trending fault systems like the Hosgri-San Gregorio (strike, N21°W), 6±8 mm/yr of right-lateral slip could be induced. Substantially, but not conclusively, VLBI eliminates the component of the San Andreas discrepancy offshore west of C. Additional observing campaigns at the Pacific Island sites will more tightly focus this picture within 2 or 3 years.

Tectonic Implications of VM2 at Point D

V_{SA}. The rate of San Andreas slip in VM2 (25.0±1.1 mm/yr) overlaps *Weldon and Sieh*'s [1985] estimate of Holocene movement (24±3 mm/yr) at Cajon Creek, northwest of D. The VM2 azimuth of interplate motion (N52°±3°W) implies a change in deformation style in traveling south to north through D. South of Palm Springs, the San Andreas trends roughly N50°W. Interplate motions near the Salton Sea would be nearly strike slip with a slight component of fault-normal tension. North of Los Angeles, the San Andreas takes a more westerly trend (N70°W) and would develop 8±1 mm/yr of fault normal compression as a consequence. Convergence across the transverse ranges may be slowing, judging from geological studies which infer crustal shortening rates of 17.6 to 26.5 mm/yr over the past 2-3 m.y. [*Namson and Davis*, 1988].

V_E. Integrated deformation along path ND (8.8±1.1 mm/yr, N25°±8°W) is similar to that found along path *NC* to central California. Note that as D moves farther to the south (Figure 4), ND will no longer traverse the borderland. The ≈9 mm/yr of motion ascribed to that portion of the path would be transferred to the southern California-North America boundary and expressed by a slip rate steadily increasing from 25 to 34 mm/yr as the San Andreas/Imperial fault system heads into Mexico. Slip rates on the Imperial fault are not well established. Local geodetic surveys from 1941 to 1978 return numbers between 30 and 40 mm/yr and do point toward higher rates compared with the values found for the San Andreas north of the Salton Sea [*Working Group on California Earthquake Probabilities*, (*WGCEP*), 1988].

V_W. VM2 finds 13.3±1.6 mm/yr (N21° ± 5°W) of deformation within the Southern California plate westward from the San Andreas. Most of the motion likely concentrates on the San Jacinto and Elsinore faults. Slip rates in the central Anza section of the San Jacinto reach 11±3 mm/yr but taper off to 8±3 mm/yr in the north and 4±1 mm/yr in the south [*WGCEP*, 1988]. *Vaughan and Rockwell* [1986] site geological evidence supporting 5 mm/yr slip on the Elsinore, however local geodetic networks do not currently show strain accumulation across the fault [*King and Savage*, 1983]. Possibly 1-5 mm/yr of motion would remain to be accommodated offshore in southern California.

Tectonic Implications of VM2 at Point E

V_{SA}. At point E along the north California coast, VM2 puts 10.6±2.1 mm/yr (N14°±11°W) of slip on the San Andreas, which here runs just offshore. VLBI contributes to the already strong evidence [e.g., *Perkins et al.*, 1989] for a nearly 50% decrease in San Andreas slip rate in moving northward from point C. In the San Francisco peninsula for instance, *Prescott et al.* [1981], *Prescott and Yu* [1986], and *Thatcher* [1979] infer slip rates in the range 8-15 mm/yr from geodetic data, although several of the estimates might be regarded as minimum values [*WGCEP*, 1988]. Along the Santa Cruz segment of the San Andreas which ruptured during the 1989 Loma Prieta earthquake, VM2 predicts an azimuth of Pacific-Northern California plate motion which is 16° easterly from the local N46°W trend of the fault. This discrepancy is consistent with a "restraining bend" interpretation for the Santa Cruz segment and with the oblique thrust mechanism observed for the earthquake [*Dietz and Ellsworth*, 1990].

V_E^2. The Hayward, Calaveras, and Rogers Creek-Healdsberg faults in the east San Franciso Bay apparently siphon off as much as 20 mm/yr of Pacific-North America motion. VM2 supports this notion and puts 29.3±2.0 mm/yr (N35°±5°W) of deformation in the Northern California plate eastward from E. (I note that to some extent, $V_E^2(\mathbf{E})$ has been artificially inflated at the expense of $V_{SA}(\mathbf{E})$ by including the Pt. Reyes VLBI station on the Northern California plate across the San Andreas from its true location. This is done because at least two vector site velocities are needed on each plate to obtain a unique Euler pole.) How deformation is distributed through the coast ranges north of San Francisco Bay is poorly understood. Unfortunately, VLBI, with only two stations in the vicinity, can not add much detail.

V_E^1. The magnitude of Basin and Range expansion along the northern NE path (8.2±1.3 mm/yr) is nearly unchanged from the rates obtained along NC and ND. The azimuth of integrated deformation (N46°±11°W) through the northern Basin and Range tends 12° and 21° more westerly than along the central and southern routes and aligns more closely with the Minster and Jordan models.

Conclusions

Expansion and densification of the VLBI network continues to clarify details of Pacific-North America motion and permits, for the first time, construction of rigid plate tectonic models based purely on space geodetic data. Construction of VLBI plate models has the advantages of averaging the bias and errors of individual site velocities, making failures in the rigid plate assumption easy to document, and allowing the consistency of specified plate models to be quantified against the VLBI data set as a whole.

Four VLBI plate models designated VM1A, VM1B, VM2, and VM3, are built in two independent steps by fitting vector velocities of 26 stations in North America and the Pacific. Step I employs the velocities of ten stations thought to be

in the rigid plate interiors to fix total Pacific-North America motion and examine plate stability. Step II employs the velocities of 16 remaining sites in the deforming borderland to find path averaged deformation along three routes from stable North America to points on the San Andreas in northern, central, and southern California. VM1A and VM1B are reference models in which the Pacific-North America pole is constrained by RM2 and NUVEL 1. VM2 frees the pole and tests RM2 and NUVEL 1 predictions. VM3 extends VM2 by permitting deformation between the western and eastern Pacific. VM3 returns Pacific-North America motion without assuming that Vandenberg and Ft. Ord are firmly fixed to the Pacific plate and tests the need for strain accumulation off of the central California coast.

The VM models document a misfit of VLBI observations and RM2 predictions at the 10 interior sites significant at the 99% confidence level. RM2 is incompatible with VLBI data even after accounting for inconsistencies resulting from the rigid plate assumption. NUVEL 1 reproduces the velocities of the 10 sites far better than RM2 and offers a fit to the data which is statistically indistinguishable from VM2 and VM3.

By including velocities of the 16 stations in the deforming plate margin, VM2 and VM3 can resolve all four terms in the vector equation (1) characterizing Pacific-North America plate boundary deformation for several points along the San Andreas without reference to a global plate model, geological or local geodetic measurements, or restrictions on distributed shear. In most cases, instantaneous VLBI-determined rates overlap geologically based estimates.

Mapped to point C in central California, VM2 finds total Pacific-North America motion of 46.8 mm/yr (N36°W). VLBI confirms and accentuates the decrease in Pacific-North America rates proposed in NUVEL 1 and in revised estimates of seafloor spreading in the Gulf of California. VM2's San Andreas slip vector (38.6 mm/yr, N36°W) differs from average Holocene motion by 5.6 mm/yr (N4°W). I associate the difference with deformation of the coast ranges to the west of C. VLBI detects 8.2 mm/yr of expansion across the Basin and Range. The rate is in accord with most geological evidence, but the direction tends 14-30° more northerly than do models by *Minster and Jordan* [1987]. The azimuth discrepancy may reflect the different nature of geological versus geodetic constrains or just be an artifact of analysis assumptions. VLBI substantially eliminates the offshore component of the San Andreas Discrepancy west of C, although a few millimeters per year of right lateral slip on fault systems like the Hosgri-San Gregorio can not be rejected.

In southern California, VM2 finds a much slower rate of San Andreas slip (25.0 mm/yr, N52°W) than along the central coast. Most of the decrease (13.3 mm/yr, N21°W) is accommodated in the southern California borderland west of the San Andreas to the Channel Islands. The azimuth of San Andreas slip suggests that the transverse ranges north of Los Angeles are absorbing 8±1 mm/yr of compression perpendicular to the trend of the fault. South of the Salton Sea, approximately 9 mm/yr of motion taken up by the Basin and Range will be transferred to the San Andreas and manifested in steadily increasing slip rates.

VLBI supports local geodetic evidence for a pronounced decrease in San Andreas slip in northern California. Between 15 and 20 mm/yr of Pacific-North America motion is siphoned off to faults east and north of the San Francisco Bay.

The capability to model secular movements of the entire Earth's land surface in real time based upon space geodetic data is becoming reality. The current capacity of the VLBI network to monitor crustal motions of the order of 2-3 mm/yr over continental baselines can already place meaningful constraints on global plate models, address questions of lithospheric stability and identify and quantify the behavior of continuous zones of deformation. Confirmation or contradiction of real time observations and geological portraits of tectonics should provide many exciting avenues of research as the VLBI network expands around the globe.

Acknowledgments. I thank Dave Gordon for supplying the VLBI data. I also thank Dave Gordon, Jeanne Sauber, Tom Jordan, Bernard Minster, Chuck DeMets, and several reviewers for their helpful suggestions. This work has been partially supported by NASA's Crustal Dynamics Project award NASA-560, National Science Foundation contract EAR 87-20328, and W. M. Keck Foundation award 892. Contribution 63, C. F. Richter Laboratory, Institute of Tectonics, University of California, Santa Cruz.

REFERENCES

Clark, T. A., D. Gordon, W. E. Himwich, C. Ma, A. Mallama, and J. W. Ryan, Determination of relative site motions in the western United States using Mark III VLBI, *J. Geophys. Res., 92*, 12,741-12,750, 1987.

Coates, R. J., H. Frey, J. Bosworth, and G. Mead, Space-age geodesy: The NASA Crustal Dynamics Project, *IEEE Trans. Geosci. Remote Sens., GE-23*, 358-368, 1985.

DeMets, C., R. G. Gordon, D. F. Argus, and S. Stein, Current Plate Motions, *Geophys. J., 101*, 425-478, 1990.

Dietz, L., and W. Ellsworth, The October 17, 1989 Loma Prieta, California, earthquake and its aftershocks: Geometry of the sequence from high-resolution locations. *Geophys. Res. Lett., 17*, 1417-1420, 1990.

Feigl, K. L., R. W. King, and T. H. Jordan, Geodetic measurement of tectonic deformation in the Santa Maria fold and thrust belt, California, *J. Geophys. Res., 95*, 2679-2699, 1990.

Greensfelder, R. W., F. C. Kintzner, and M. R. Somerville, Seismotectonic regionalization of the Great Basin, and comparison of moment rates computed from Holocene strain and historic seismicity, *Geol. Soc. Am. Bull., 91*, 518-523, 2039-2111, 1980.

Gordon, D., and J. Sauber, Geodesy by radio interferometry: Determination and analysis of vector site motions in the southwestern United States, (abstract),*Eos, Trans. AGU*, 1988.

Gordon, D., C. M. Ma., T. A. Clark, and J. W. Ryan, Site velocities from the Crustal Dynamics Project VLBI geodynamics database, (abstract), *Eos, Trans. AGU*, 1988.

King, N. E., and J. C. Savage, Strain rate profile across the Elsinore, San Jacinto, and the San Andreas faults near Palm Springs, California, *Geophys. Res. Lett., 10*, 55-57, 1983.

Millman, D. E., and T. K. Rockwell, Lateral offset of mid- and late Quaternary deposits along the northern Elsinore fault, southern California (abstract), *Geol. Soc. Am. Abstr. Programs, 17*, 370, 1985.

Minster, J. B., and T. H. Jordan, Present-day plate motions, *J. Geophys. Res., 83*, 5331-5354, 1978.

Minster, J. B., and T. H. Jordan, Vector constraints on quaternary deformation of the western United States east and west of the San Andreas fault, in *Tectonics and Sedimentation along the California Margin*, Publ. 38, edited by J. K. Crouch and S. B. Bachman, *Pacific Section Society of Economic Paleontologists and Mineralogists*, pp. 1-16, Bakersfield, Calif., 1984.

Minster, J. B., and T. H. Jordan, Vector constraints on western U.S. deformation from space geodesy, neotectonics, and plate motions, *J. Geophys. Res.*, 92, 4798-4804, 1987.

Namson, J., and T. Davis, Structural transect of the western Transverse Ranges, California: Implications for lithospheric

kinematics and seismic risk evaluation, *Geology, 16*, 675-679, 1988.

Perkins, J. A., J. D. Sims, and S. S. Sturgess, Late Holocene movement along the San Andreas fault at Melendy Ranch: Implications for the distribution of fault slip in central California, *J. Geophys, Res., 94*, 10,217-10,230, 1989.

Prescott, W. H., and S. B. Yu, Geodetic measurement of horizontal deformation in the northern San Francisco Bay region, California, *J. Geophys. Res., 91*, 7475-7484, 1986.

Prescott, W.H., M. Lisowski, and J. C. Savage, Geodetic measurement of crustal deformation on the San Andreas, Hayward, and Calaveras faults near San Francisco, California, *J. Geophys. Res., 86*, 10,853-10,869, 1981.

Savage, J.C., and R. O. Burford, Geodetic determination of relative plate motion in central California, *J. Geophys. Res., 78*, 832-845, 1973.

Sieh, K. E., and R. H. Jahns, Holocene activity of the San Andreas fault at Wallace Creek, California, *Geol. Soc. Am. Bull., 95*, 883-896, 1984.

Thatcher, W., Systematic inversion of geodetic data in central California, *J. Geophys. Res., 84*, 627-632, 1979.

Thompson, G. A., and D. B. Burke, Rate and direction of spreading in Dixie Valley, Basin and Range Province, Nevada, *Geol. Soc. Am. Bull., 84*, 627-632, 1973.

Vaughan, P., and T. Rockwell, Alluvial stratigraphy and neotectonics of the Elsinore fault zone at Aqua Tibia Mountain, southern California: in Ehlig, P.L., compiler, Neotectonics and faulting in southern California, Guidebook and Volume, Cordilleran Section, *Geol. Soc. Am.*, 177-191, 1986.

Wallace, R. E., Patterns of faulting and seismic gaps in the Great Bas province, Proceedings of Conference VI, Methodology for Identifying Seismic Gaps and Soon-to-Break Gaps, *U.S. Geol. Surv. Open File Rep., 78*, 943, 1978.

Ward, S. N., North America-Pacific plate boundary, an elastic-plastic megashear, evidence from very long baseline interferometry, *J. Geophys. Res., 93*, 7716-7728, 1988.

Weldon, R. J., and K. E. Sieh, Holocene rate of slip and tentative recurrence interval for large earthquakes on the San Andreas fault in Cajon Pass, southern California, *Geol. Soc. Am. Bull., 96*, 793-812, 1985.

Working Group on California Earthquake Probabilities, Probabilities of large earthquakes occurring in California on the San Andreas fault, *U.S. Geol. Surv. Open File Rep., 88-398*, 1988.

Zoback, M. L., and M. D. Zoback, Faulting patterns in north central Nevada and strength of the crust, *J. Geophys. Res., 85*, 275-284, 1980.

S. N. Ward, C. F. Richter Laboratory, Institute of Tectonics, University of California, Santa Cruz, CA 96064.

(Received November 17, 1989;
revised May 21, 1990;
accepted July 23, 1990.)